iScience

CellPress

Article

NCoR1: Putting the Brakes on the Dendritic Cell Immune Tolerance

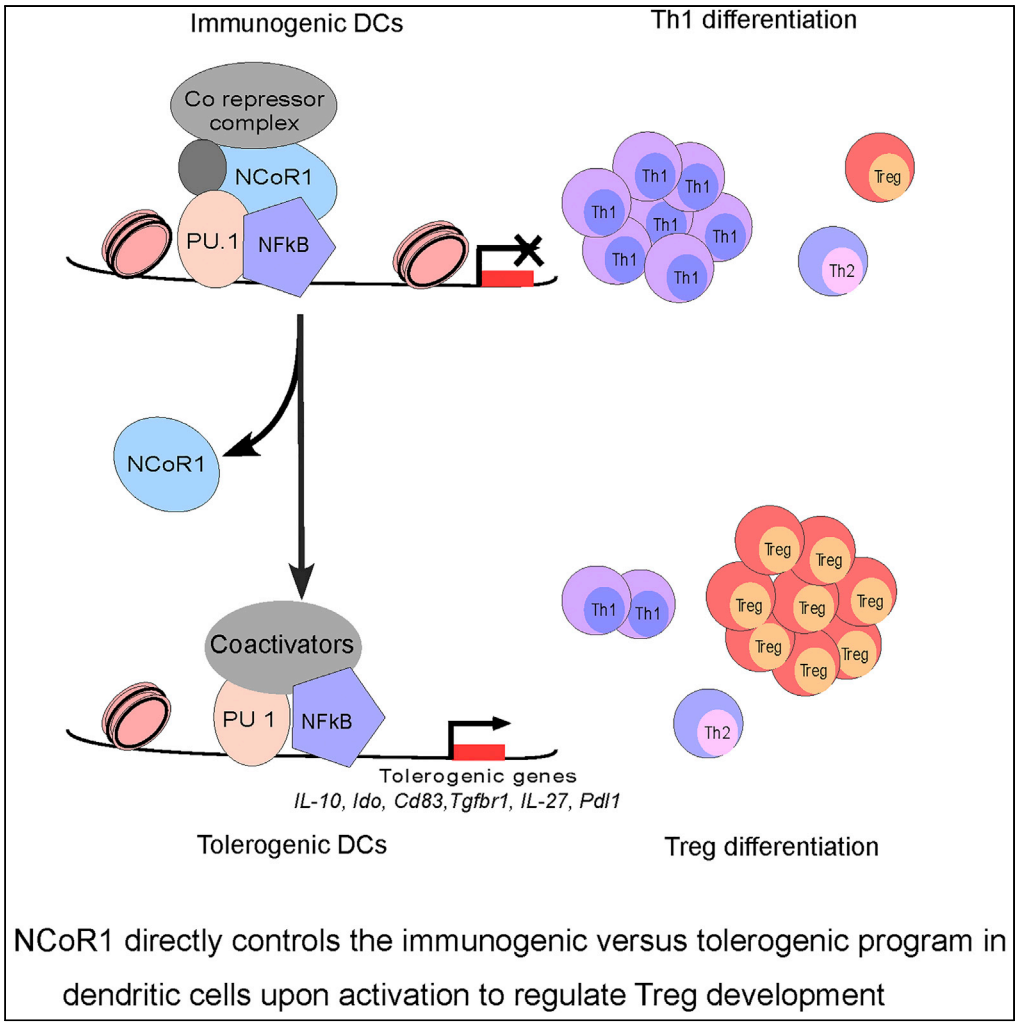

NCoR1 directly controls the immunogenic versus tolerogenic program in dendritic cells upon activation to regulate Treg development

Abdul Ahad, Mathias Stevanin, Shuchi Smita, ..., Bhawna Gupta, Hans Acha-Orbea, Sunil Kumar Raghav

hans.acha-orbea@unil.ch (H.A.-O.)
sunilraghav@ils.res.in (S.K.R.)

HIGHLIGHTS

NCoR1 directly represses tolerogenic program in mouse cDCs

Depletion of NCoR1 in cDCs enhanced Treg development *ex vivo* and *in vivo*

NCoR1 masks PU.1-bound super-enhancers on tolerogenic genes in cDCs

NCoR1$^{DC-/-}$ animals depicted enhanced Treg frequency and infection load

Ahad et al., iScience *19*, 996–1011
September 27, 2019
https://doi.org/10.1016/j.isci.2019.08.024

iScience

CellPress

Article

NCoR1: Putting the Brakes on the Dendritic Cell Immune Tolerance

Abdul Ahad,[1,2,7] Mathias Stevanin,[3,7] Shuchi Smita,[1,2,7] Gyan Prakash Mishra,[1,6] Dheerendra Gupta,[1] Sebastian Waszak,[4] Uday Aditya Sarkar,[5] Soumen Basak,[5] Bhawna Gupta,[6] Hans Acha-Orbea,[3,*] and Sunil Kumar Raghav[1,2,6,8,*]

SUMMARY

Understanding the mechanisms fine-tuning immunogenic versus tolerogenic balance in dendritic cells (DCs) is of high importance for therapeutic approaches. We found that NCoR1-mediated direct repression of the tolerogenic program in conventional DCs is essential for induction of an optimal immunogenic response. NCoR1 depletion upregulated a wide variety of tolerogenic genes in activated DCs, which consequently resulted in increased frequency of FoxP3^{+} regulatory T cells. Mechanistically, NCoR1 masks the PU.1-bound super-enhancers on major tolerogenic genes after DC activation that are subsequently bound by nuclear factor-κB. NCoR1 knockdown (KD) reduced RelA nuclear translocation and activity, whereas RelB was unaffected, providing activated DCs a tolerogenic advantage. Moreover, NCoR1$^{DC-/-}$ mice depicted enhanced Tregs in draining lymph nodes with increased disease burden upon bacterial and parasitic infections. Besides, adoptive transfer of activated NCoR1 KD DCs in infected animals showed a similar phenotype. Collectively, our results demonstrated NCoR1 as a promising target to control DC-mediated immune tolerance.

INTRODUCTION

Dendritic cells (DCs) are specialized antigen-presenting cells (APCs) that link innate to adaptive immunity (Steinman, 2006). Upon encounter with pathogens, they get activated resulting in maturation and migration to draining lymph nodes. Primed DCs then polarize naive and memory T helper (Th) cells into various effector subtypes such as Th1, Th2, Th17, or Tregs (Hochweller et al., 2010; Kapsenberg, 2003). The differentiation of these different Th subsets depends on the DC maturation status and the secreted cytokines. DCs are thus considered as major players in fine-tuning immunity versus immune tolerance.

DCs express a range of pattern recognition receptors such as Toll-like receptors (TLRs) to identify a wide plethora of pathogens (Takeuchi and Akira, 2010). Here in this study, we have focused mostly on CD8^{+} cDC1 DCs. cDC1 DCs are the main antigen cross-presenting DCs for intracellular pathogens detected through TLR3 and TLR9 (Reizis, 2011; Schnorrer et al., 2006). Upon ligation of these receptors, Myd88 and TRIF signaling pathways are stimulated, consequently activating transcription factors (TFs) like nuclear factor (NF)-κB and interferon regulatory factors (IRFs) and a variety of protein kinases (Kawasaki and Kawai, 2014; O'Neill et al., 2013). It has been reported that in DCs canonical NF-κB signaling through IkBα activates both RelA and RelB, whereas in other cells like fibroblasts only non-canonical signaling results in RelB activation (Shih et al., 2012). RelA signaling is important for pro-inflammatory response and cell survival (Shih et al., 2012). On the other side, RelB is reported to be involved in DC maturation and induction of tolerance (Azukizawa et al., 2011; Thomas, 2013). Therefore depending on the stimulus and a fine balance of NF-κB activity, DCs exhibit either immunogenic or regulatory phenotype (Vendelova et al., 2018). The activation stimulus results in signal-specific expression of a large number of DC response genes including cytokines (interleukin [IL]-6, IL-10, IL-12) and co-stimulatory markers (CD40, CD80, and CD86) (Matsushima et al., 2004). Depending on the strength and specificity of these DC responses, naive Th cells differentiate into different effector subtypes (Hochweller et al., 2010; Kaiko et al., 2008). The inflammatory cytokine IL-12 with strong co-stimulatory signals results in Th1, whereas anti-inflammatory signals IL-4, IL-5, and IL-13 induce Th2 development (Liu et al., 2005b) (MacDonald and Maizels, 2008). Similarly, the cytokine IL-10, with strong or weak co-stimulatory signals, respectively, generates Th2 or Tregs (Couper et al., 2008; Saraiva and O'Garra, 2010). Thus, it has been widely proposed that DC responses can be modulated to treat a variety of diseases, such as cancer and autoimmunity (Moreau et al., 2017).

[1]Immuno-genomics & Systems Biology Laboratory, Institute of Life Sciences (ILS), Bhubaneswar, Odisha 751023, India

[2]Manipal Academy of Higher Education, Manipal, Karnataka 576104, India

[3]Department of Biochemistry CIIL, University of Lausanne (UNIL), Epalinges CH-1066, Switzerland

[4]European Molecular Biology Laboratory (EMBL), Heidelberg 69117, Germany

[5]Systems Immunology Laboratory, National Institute of Immunology (NII), Aruna Asaf Ali Marg, New Delhi 110067, India

[6]Department of Biotechnology, Kalinga Institute of Industrial Technology (KIIT), Bhubaneswar, Odisha 751024, India

[7]These authors contributed equally

[8]Lead Contact

*Correspondence: hans.acha-orbea@unil.ch (H.A.-O.), sunilraghav@ils.res.in (S.K.R.)

https://doi.org/10.1016/j.isci.2019.08.024

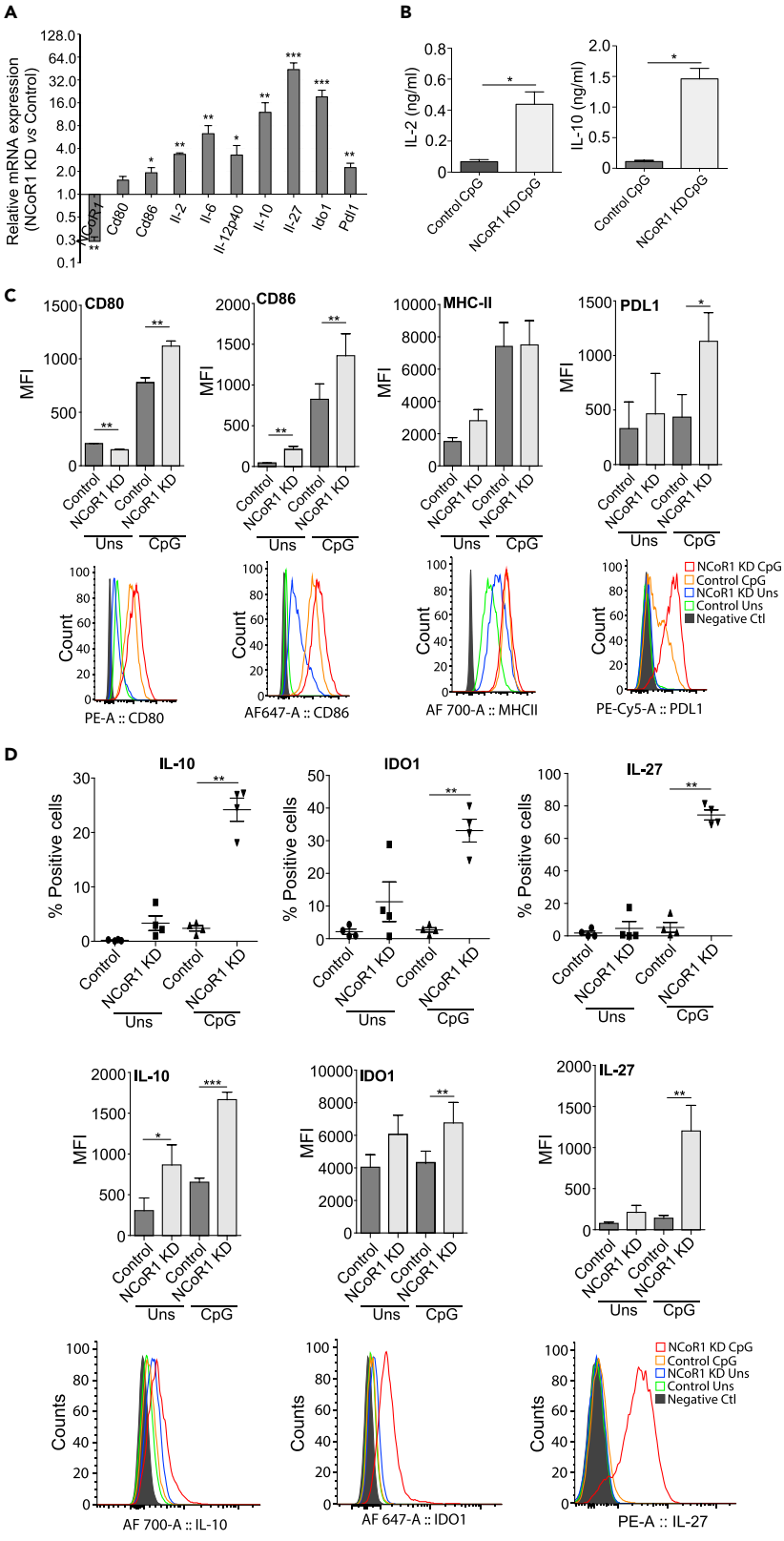
A
Relative mRNA expression (NCoR1 KD vs Control)
128.0
64.0
32.0
16.0
8.0
4.0
2.0
1.0
0.5
0.3
0.1
Ncor1
Cd80
Cd86
Il-2
Il-6
Il-12p40
Il-10
Il-27
Ido1
Pdl1
B
IL-2 (ng/ml)
IL-10 (ng/ml)
Control CpG
NCoR1 KD CpG
C
CD80
CD86
MHC-II
PDL1
MFI
Control
NCoR1 KD
Uns
CpG
Count
PE-A :: CD80
AF647-A :: CD86
AF 700-A :: MHCII
PE-Cy5-A :: PDL1
NCoR1 KD CpG
Control CpG
NCoR1 KD Uns
Control Uns
Negative Ctl
D
IL-10
IDO1
IL-27
% Positive cells
Counts
AF 700-A :: IL-10
AF 647-A :: IDO1
PE-A :: IL-27

Figure 1. NCoR1 KD Enhances Tolerogenic Responses in Conventional DCs upon CpG Challenge

(A) Bar plot depicting the transcript expression of selected immunogenic and tolerogenic response genes in 6 h CpG-stimulated NCoR1 KD cDC1 DCs relative to control cells as quantified by qPCR (n = 3).

(B) Bio-Plex quantitation of the secreted cytokines IL-2 and IL-10 in the culture supernatants of 6 h CpG-challenged NCoR1 KD and control DCs (n = 6).

(C) Graph demonstrating the MFI for DC activation and co-stimulation markers CD80, CD86, MHC-II, and PDL1 in NCoR1 KD and control cDC1 DCs before and after 6 h CpG challenge. Corresponding histogram plot is a representative plot for MFI shifts observed for respective markers (n = 4–8).

(D) Scatterplot showing the percentage positive cells for intracellular expression of IL-10, IDO1, and IL-27 in 0 h and 6 h CpG-stimulated NCoR1 KD and control cDC1 line. Corresponding bar plot and histogram show the MFI shifts observed for the respective genes (n = 4).

p values are calculated using two-tailed paired Student's t test; error bars represent SEM. *$p \leq 0.05$, **$p \leq 0.01$, ***$p \leq 0.001$. See also Figures S1 and S2.

We know that DCs receive multiple stimulatory cues to generate signal-specific responses, and it appears improbable that TFs alone can integrate such a vast number of regulatory signals. One of the well-characterized mechanisms how nuclear receptors (NRs) regulate transcriptional responses is through the recruitment of transcriptional co-regulators (co-repressors or co-activators) (McKenna and O'Malley, 2002; Mouchiroud et al., 2014; Ng et al., 2011). Recent reports show that DC treatment with high-affinity NR ligands such as rosiglitazone and vitamin D modulates expression of co-stimulatory molecules and cytokine genes, which perturbs their functional responses (Agrawal et al., 2016; Farias et al., 2013; Thompson et al., 2007). Analysis of published NCoR1 chromatin sequencing (ChIP-seq) data from macrophages revealed NCoR1 binding on genes accountable for antigen recognition, co-stimulation, and T cell polarization in DCs. This strongly suggested the functional involvement of NR co-repressors like NCoR1 in DCs, as they were identified in complexes with unliganded NRs such as peroxisome proliferator activated receptor gamma (PPARγ) and thyroid receptor (TR) (Cohen et al., 1998; Huang et al., 2009; Li et al., 2013; Mottis et al., 2013; Yu et al., 2005). These co-repressors inhibit gene expression through chromatin compaction by recruiting histone deacetylases (Huang et al., 2009; Perissi et al., 2008). In contrast, we reported NCoR1 enrichment at open chromatin regions marked by H3K27ac/H3K4me1 (Raghav et al., 2012). Despite several reports indicating so, a role of NCoR1 in DC function has not been directly evaluated in a systematic study.

Here, we employed an immunogenomics approach to elucidate the role of NCoR1 in DC function. We demonstrated NCoR1 as a master regulator of the tolerogenic program in cDCs. We found that direct repression of tolerogenic genes by NCoR1 upon DC activation is important to induce an optimal immunogenic response. In addition, we explored the underlying molecular mechanisms and *in vivo* physiological impact of NCoR1-modulated DC responses in parasite-infected animals.

RESULTS

NCoR1 KD cDC Line Showed Enhanced Tolerogenic Responses upon Activation

To determine the role of NCoR1 in DCs, we have developed a stable NCoR1 knockdown (KD) and matched empty vector-transduced control cells using lentiviral short hairpin RNA (shRNA) approach in a CD8α$^+$ cDC1 DC line that mimics remarkably the *ex vivo* isolated cDC1 DCs (Fuertes Marraco et al., 2012; Smita et al., 2018). We found that NCoR1 transcript levels were significantly reduced (≥85%) in NCoR1 shRNA-transduced DCs (Figures 1A and S1A). We first performed qPCR-based immune profiling of control and NCoR1 KD DCs. We found that NCoR1 depletion significantly increased transcripts of several immune-modulatory genes including *Il-10, Il-12p40, Il-27, Ido1,* and *Pdl1* upon 2-, 6-, and 12-h CpG challenge (Figures 1A and S1A). The luminex assay showed significantly increased secretion of IL-2, IL-6, and IL-10 cytokines in the culture supernatants of 6-h CpG-activated NCoR1 KD DCs, whereas the IL-12 cytokine was insignificantly increased (Figures 1B and S1B). The median fluorescence intensity (MFI) shifts showed a significant decrease of CD80 in unstimulated conditions, whereas upon CpG activation CD80, CD86, major histocompatibility complex (MHC)-I, and PDL1 expression were significantly increased (Figures 1C and S1C). CD40 and MHC-II remain unchanged in both the conditions (Figures 1C and S1C). Moreover, the intracellular expression of IL-6, IL-10, IDO1, and IL-27 cytokines showed significantly increased levels in 6-h CpG-challenged NCoR1 KD DCs, whereas IL-12p40 showed an insignificant increase (Figures 1D and S1D). The expression of *IL-10* is predominantly dependent on Erk kinase activity (Saraiva and O'Garra, 2010). We found significantly increased pErk$^+$IL-10$^+$pSTAT3$^-$ cells in activated NCoR1 KD DCs (Figure S1E).

Moreover, we also developed a stable NCoR1 KD CD11b$^+$ cDC2 DC line (Pigni et al., 2018). Similar to cDC1 DCs, we identified a significantly increased percentage of positive cells for IL-10, IL-27, PDL1, IL-6, and

IL-12p40 cytokines after CpG activation in NCoR1-depleted DCs (Figure S1F). Lipopolysaccharide challenge showed similar trends (Figure S1F).

At the same time, to identify if any strong stimulation renders similar responses in NCoR1-depleted cDCs, we challenged NCoR1 KD and matched control cDC1 DCs with pIC (TLR3) and CpG + pIC (TLR3 and TLR9 together) simultaneously. We found that NCoR1 depletion enhanced expression of IL-10, IL-27, IDO-1, and PDL1 along with IL-6 and IL-12p40 in cDC1 DC line with both these stimulations (Figure S2A). Moreover, simultaneous activation showed stronger DC responses (Figure S2A). We also challenged NCoR1 KD and control CD8α^+cDC1 DCs with gram-positive (*Mycobacterium smegmatis, B. subtilis* and *Staphylococcus aureus*), and gram-negative (*Vibrio cholerae, Shigella dysenteriae,* and *Salmonella typhimurium*) bacteria. Interestingly, we found a profound increase of IL-10, IL-27, IDO1, CTLA4, and PDL1 in NCoR1 KD DCs in all these stimulations (Figures S2B and S2C).

Indoleamine 2,3-dioxygenase (IDO) enzyme metabolizes L-tryptophan to L-kynurenine resulting in the inhibition of effector Th cell differentiation (Yan et al., 2010). We found a significantly increased IDO activity in the culture supernatants of NCoR1 KD DCs when compared with controls (Figure S1G). This further substantiated our observation that NCoR1 directly controls the tolerogenic program in cDCs upon activation. Several recent reports showed an enhanced expression of IL-10 along with PDL1, IL-27, and IDO1 in tolerogenic DCs (Kowalczyk et al., 2014; Mellor and Munn, 2004; Tsoumakidou et al., 2014; Yoo and Ha, 2016). Collectively, we demonstrated that NCoR1 depletion induces strong tolerogenic response upon activation in cDCs.

NCoR1 KD cDC1 DCs Increased Frequency of Treg Development *Ex Vivo*

To access the impact of NCoR1 depletion in cDCs on Th cell differentiation, we co-cultured NCoR1 KD and control cDC1 DCs with naive CD4$^+$ Th cells isolated from OT-II mice (Figure 2A). We found profoundly increased proliferation of Th cells co-cultured with CpG-pulsed NCoR1 KD DCs when compared with control cells (Figure 2B). In addition, the differentiation profile showed a significantly higher number of CD25^{+}-FoxP3$^+$ Tregs in NCoR1-depleted conditions (Figure 2C). Tbet and interferon (IFN)-γ-positive cells were significantly reduced, whereas GATA3 showed an increasing trend (Figure 2D) The MFI shifts showed similar trends (Figure 2C). In unstimulated conditions, no changes were observed (Figure 2D). These results confirmed the tolerogenic potential of activated NCoR1 KD cDC1 DCs.

Conventional DCs from NCoR1$^{DC-/-}$ Mice Showed Increased Tolerogenic Responses upon CpG Challenge

To validate the findings *in vivo*, we developed DC-specific conditional NCoR1 knockout mice by crossing CD11c-Cre strains with floxed NCoR1 mice (Yamamoto et al., 2011). Genotyping PCR confirmed NCoR1 ablation in CD11c$^+$ cDCs (Figure S3A). To obtain sufficient numbers of DCs *ex vivo* from NCoR1$^{DC-/-}$ and wild-type (WT) mice, we treated them with serum from FLT3L transgenic mice (equivalent to 50 μg FLT3L/mouse/day) for eight consecutive days (Baerenwaldt et al., 2016). First, we profiled DC subtype composition (cDCs and pDCs) after FLT3L treatment. We found that the frequencies of CD8$^+$ (cDC1) and CD11b$^+$ cDCs (cDC2) were profoundly increased in FLT3L-treated mice (Figures S3B and S3C). Then, splenocytes from NCoR1$^{DC-/-}$ and WT mice were stimulated for 6 h with or without CpG and analyzed by fluorescence-activated cell sorting (FACS) to identify the impact of NCoR1 ablation on different subsets of primary CD11c$^+$ cDCs (Figure S3D). We found that NCoR1 loss in CD11c^{high}CD8$^+$ cDC1 DCs significantly enhanced the percentage positive cells of IL-10, IL-27, and IDO1 after activation, whereas IL-6 showed a marginal but insignificant increase (Figure 3A). The MFI shifts showed similar trend (Figure 3A). In addition, CD11b$^+$ cDC2 DCs also showed a significant increase of IL-27 and IDO1 in NCoR1$^{DC-/-}$ when compared with WT mice, whereas IL-6 and IL-10 exhibited an increasing trend (Figures 3B and S3E). Surface expression of CD80 was significantly decreased upon NCoR1 loss of function in both CD8$^+$ and CD11b$^+$ primary cDCs in unstimulated conditions (Figures 3C and 3D). No significant differences were observed for other co-stimulatory genes CD40, CD86, and MHC-II (Figures S3F and S3G). As we found an increased expression of IL-2 cytokine in DC line, we analyzed it in primary DCs using FACS. We found significantly higher IL-2-positive cells in both cDC1 (CD8$^+$) and cDC2 DCs (CD11b$^+$) in CpG-challenged NCoR1-ablated condition (Figure S3I).

OVA Immunization Enhances Tregs Frequency in NCoR1$^{DC-/-}$ Mice

To access the *in vivo* impact of NCoR1 deletion in cDCs on Th cell differentiation, we vaccinated NCoR1$^{DC-/-}$ and WT mice with ovalbumin (OVA) and CpG at D0 followed by a booster immunization after 30 days (Figure 3E). Three days after the booster injection, draining lymph nodes were harvested and

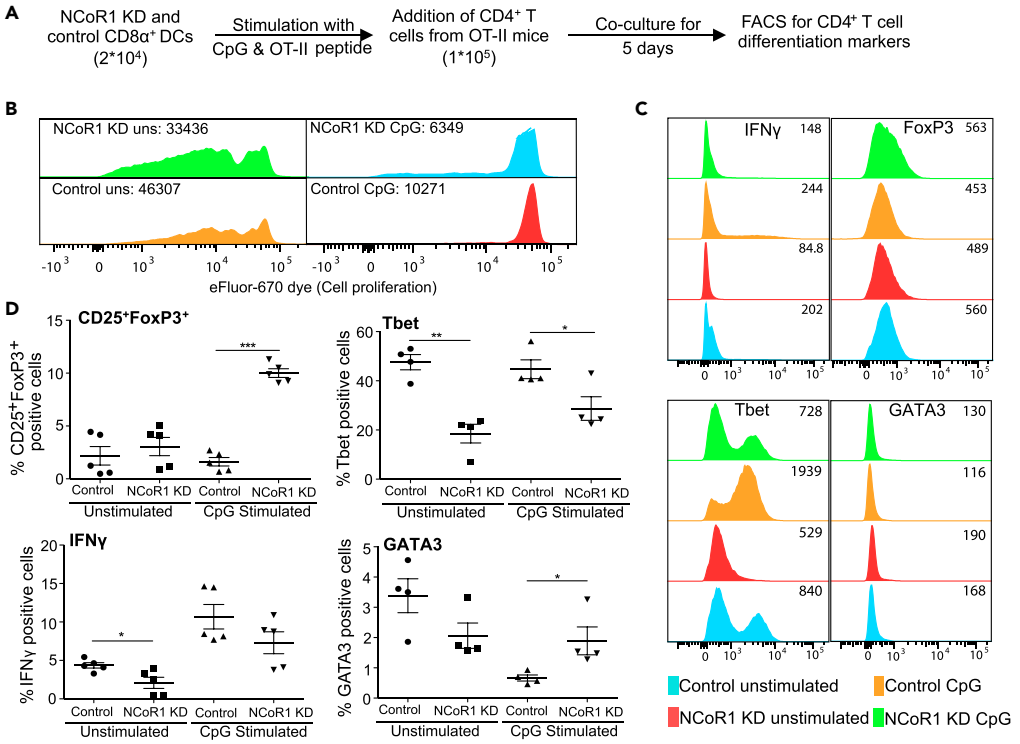

Figure 2. NCoR1 Depletion Enhances Differentiation of Naive CD4$^+$ Th Cells into Tregs

(A) Experimental outline used to assess the effects of NCoR1 KD on T cell polarization *ex vivo*.

(B) Representative histograms showing the MFI shifts observed for proliferation of T helper cells co-cultured with unstimulated or CpG-activated NCoR1 KD and control cDC1 DCs (n = 3).

(C) Histogram plots demonstrating the representative MFI shifts observed for FoxP3, Tbet, IFNγ, and GATA3 in helper T cells co-cultured with NCoR1 KD and control cDC1 DCs for 5 days (n = 5).

(D) Scatterplots from flow cytometric analysis showing the percentage positive T helper cells expressing CD25$^+$FoxP3$^+$, Tbet, IFNγ, and GATA3 after 5 days of co-culture with activated NCoR1 KD and control DCs (n = 5).

p values are calculated using two-sample unpaired Student's t test; error bars represent SEM. *$p \leq 0.05$, ***$p \leq 0.001$.

restimulated with PMA/ionomycin. CD3$^+$CD4$^+$CD44$^+$ effector Th cells were analyzed to assess the differentiation patterns (IFNγ for Th1, IL-13 for Th2, FoxP3 for Tregs, and IL-17 for Th17). We found significantly higher percentages of FoxP3$^+$ cells in NCoR1$^{DC-/-}$ when compared with WT mice (Figure 3F). On the other side, we did not find any change in the IFNγ-, IL-13-, and IL-17-expressing cells in the analyzed effector Th population (Figure S3H). To further check the OVA-specific T cell responses, we also restimulated lymph node cells with OVA-pulsed DCs for 72 h. We found an increased proliferation of effecter Th cells in both WT and NCoR1$^{DC-/-}$ mice when compared with PBS controls (Figure S4A). At the same time, we found a robust and significantly increased FoxP3$^+$ Treg population in CD3$^+$CD4$^+$CD44$^+$ Th cells from NCoR1$^{DC-/-}$ when compared with WT mice (Figures S4A and S4B). These experiments confirmed the development of OVA-specific immune responses in both WT and NCoR1$^{DC-/-}$-immunized animals.

Moreover, we performed ELISA to evaluate OVA-specific antibody titers in immunized NCoR1$^{DC-/-}$ and WT animals to confirm the development of OVA-specific responses. We assayed OVA-specific total IgG and its subtypes IgG1, IgG2a, IgG2b, and IgG3. We found high titers of OVA-specific total IgG in both WT and NCoR1$^{DC-/-}$ animals immunized with OVA + CpG when compared with PBS controls (Figure S4C). We did not observe any significant difference in total IgG levels as well as IgG1, IgG2a, IgG2b, and IgG3 between WT and NCoR1$^{DC-/-}$ mice (Figure S4C).

NCoR1 Loss in cDC1 DCs Enhances Treg Development and Parasite Burden

To explore the *in vivo* implications, we further investigated if NCoR1 KD activated DCs can be adoptively transferred at precise time points to skew T cell polarization into Tregs and the associated disease

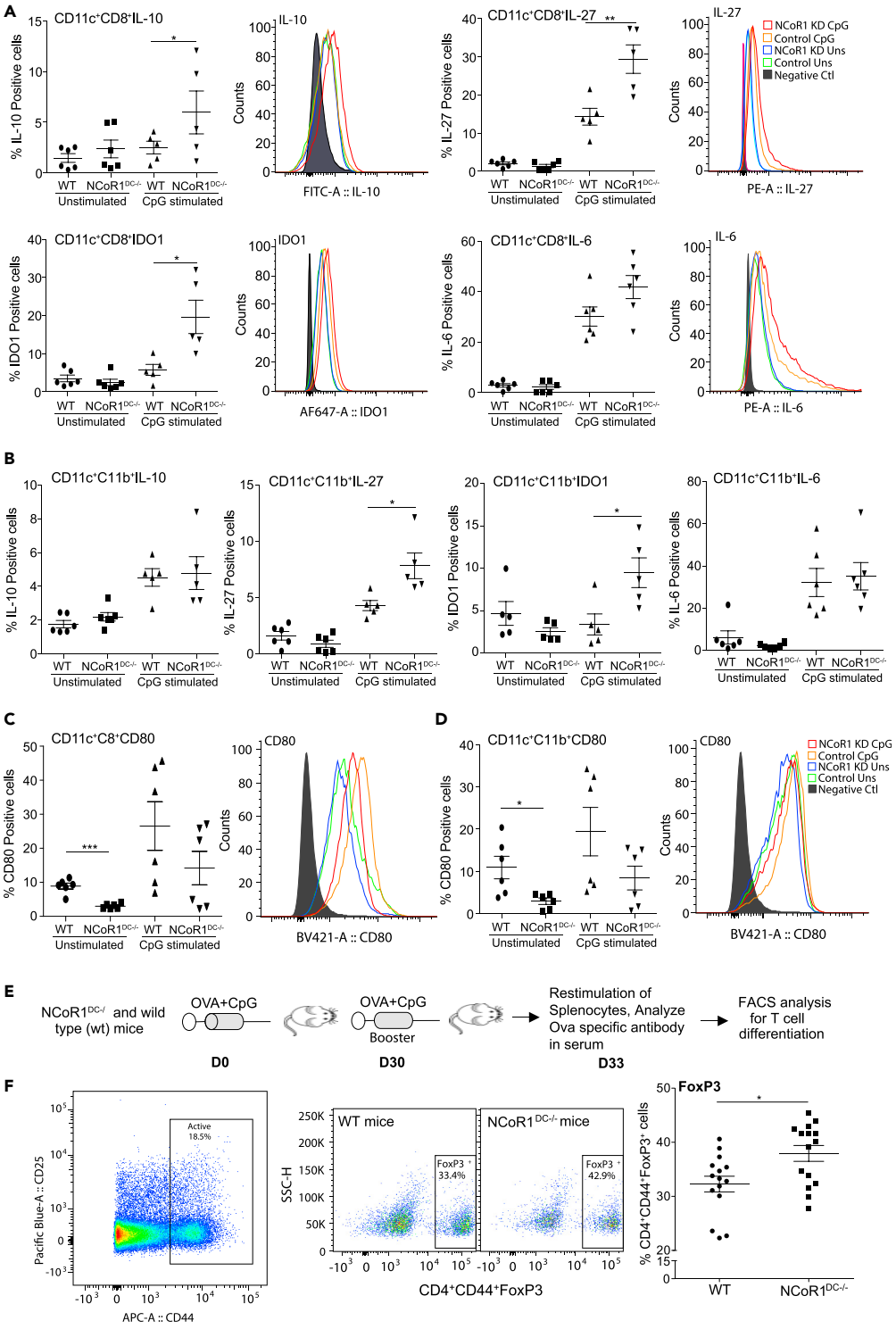

Figure 3. Conventional DCs from NCoR1$^{DC-/-}$ Mice Show Increased Tolerogenic Behavior upon Activation

Splenocytes from NCoR1$^{DC-/-}$ and WT mice were treated with and without CpG for 6 h and the impact of NCoR1 ablation on different DC subsets was analyzed by flow cytometry.

(A) Scatterplots depicting the percentage positive cells for IL-10, IL-27, IDO1, and IL-6 in primary cDC1 DCs from NCoR1$^{DC-/-}$ and WT mice. Corresponding histogram plots depict the MFI shifts (n = 6).

Figure 3. *Continued*

(B) Scatterplots demonstrating the percentage positive cells for IL-10, IL-27, IDO1, and IL-6 in primary cDC2 DCs from NCoR1$^{DC-/-}$ and WT mice (n = 6).

(C) and (D) Scatterplot showing the percentage of CD80-positive cells in primary cDC1 and cDC2 DCs respectively from NCoR1$^{DC-/-}$ and WT mice before and after 6 h CpG activation. Representative histograms depict the MFI shift.

(E) Experimental outline depicting the method employed to identify the *in vivo* impact of NCoR1 depletion on CD4$^+$ T cell polarization in NCoR1$^{DC-/-}$ and WT mice.

(F) Dot plots showing the percentage of CD4$^+$CD44$^+$FoxP3$^+$-expressing effector T cells from the draining inguinal lymph nodes of NCoR1$^{DC-/-}$ and WT mice vaccinated with CpG and OVA for 1 month (n = 15).

p values are calculated using two-tailed unpaired Student's t test; error bars represent SEM. *p $\leq$ 0.05, **p $\leq$ 0.01. See also Figures S3 and S4.

phenotypes. We employed a well-established helminth infection (*Heligmosomoides polygyrus)* model in C57BL/6 mice (Filbey et al., 2014). It is reported that the enhanced Treg population in mesenteric lymph nodes (MLNs) increases worm loads in the intestine (Taylor et al., 2012).

Adoptive transfer of CpG-pulsed NCoR1 KD cDC1 DC line at (Day 10) D10 post helminth infection in mice resulted in significantly increased egg counts at D13 and D14 post-infection (Figure 4A). The excreted egg numbers were found to be consistently higher as measured until D18. In addition, the intestinal worm load was also observed to be significantly higher in NCoR1-depleted cDC1-treated animals (Figures 4B and S5A). Besides, NCoR1 KD cDC-treated mice depicted a profound increase in FoxP3$^+$ effector Th cells in the MLNs when compared with controls (Figures 4C and S5B). No differences were observed in Tbet$^+$ cells, whereas GATA3$^+$ cells were also significantly increased (Figure S5C).

To validate our adoptive transfer observations *in vivo* in NCoR1$^{DC-/-}$ animals, we infected the NCoR1$^{DC-/-}$ and WT mice with helminth larvae and treated the animals with CpG at D10 post-infection. We found a significantly increased helminth egg load at D17 in the feces of NCoR1$^{DC-/-}$ mice compared with WT animals (Figure 4D). The intestinal worm counts were also increased (Figure 4E). In addition, the effector CD44$^+$ Th cell profiling from MLNs of infected animals showed an increased FoxP3$^+$ population in NCoR1-ablated mice (Figure 4F). We did not find any significant differences in the GATA3 and Tbet-expressing Th cells (Figure S5D). We also developed a *Leishmania major* parasitic infection model. After subcutaneous injection of *parasite* in the right footpad of NCoR1$^{DC-/-}$ and WT mice, paw thickness was monitored before and after CpG challenge. As cross-presenting DCs are essential for developing immune protection against *L. major* between 17 and 19 days (Ashok et al., 2014), mice were treated with CpG at day 18 post-infection. We observed a significantly increased (p value $\leq$ 0.020) foot inflammation at day 21 post infection in NCoR1$^{DC-/-}$ animals when compared with WT mice (Figure 4G). Although the NCoR1$^{DC-/-}$ mice had thicker paws than the WT mice, the differences disappeared 2 weeks after the CpG injection (Figure 4G). Draining lymph nodes from NCoR1$^{DC-/-}$ mice also showed significant increase in FoxP3$^+$ Th cells (Figure 4H). These results indicated a strong potential of NCoR1 in inducing Th cell polarization toward Tregs *in vivo* and modulating the underlying disease phenotype. Next, to assess the specificity of antigen presentation of DCs, we injected carboxyfluorescein succinimidyl ester (CFSE) labeled CD45.1$^+$ OT-II T cells intravenously in CD45.2$^+$ helminth-infected WT and NCoR1$^{DC-/-}$ mice at D12 of infection. Next day, we injected WT DCs pulsed with or without OVA peptide intravenously, and the animals were kept further for 3 days. Then we harvested the splenocytes to check the OVA-specific proliferation of CD45.1-gated cells. We observed no difference in proliferation of CD45.1$^+$ OT-II T cells analyzed from WT and NCoR1$^{DC-/-}$ mice suggesting there were similar levels of antigen presentation in both WT and NCoR1$^{DC-/-}$ mice (Figure S5E).

Global Profiling of NCoR1 Identifies Its Direct Control on DC Tolerogenicity

To characterize the molecular mechanisms underlying NCoR1 depletion mediated tolerogenic behavior in cDC1 DCs, we performed RNA sequencing (RNA-seq) analysis of NCoR1 KD and control cDC1 DC line at 0h and 6h after CpG challenge. Besides, we also performed ChIP-seq profiling of NCoR1 in WT cDC1 DC line in similar conditions. We identified $\approx$13,000 genomic regions bound by NCoR1 at both 0 and 6 h after CpG activation (Table S1). In addition, we performed ChIP-qPCR for 10 randomly selected NCoR1 peaks to validate the ChIP-seq data (Figure S6A, Table S1). Transcriptome profiling of NCoR1 KD cDC1 line identified 1,099 upregulated in contrast to 537 downregulated genes when compared with control DCs (q-value $\leq$ 0.05 and 2-fold) (Figure 5A, Table S2). On the other side, in unstimulated conditions, only 390 and 360 genes were up- and downregulated, respectively, in NCoR1 KD DCs (Figure 5A, Table S3). Overlap

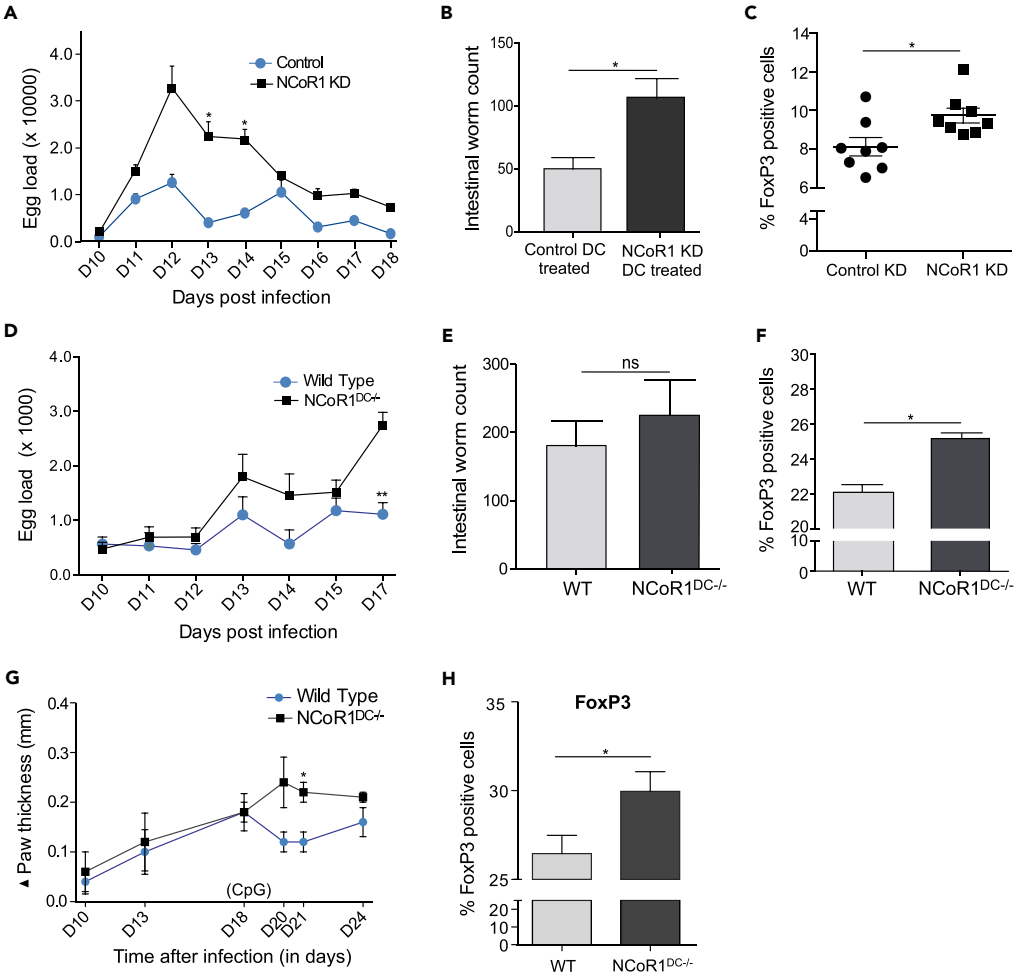

Figure 4. NCoR1 Loss in cDCs Enhances Treg Frequency *In Vivo* Leading to Increased Disease Burden in Mice

(A) Line graph demonstrating the egg loads in the feces of *H. polygyrus*-infected C57BL/6J mice at different days post-helminth infection after treatment with CpG-pulsed NCoR1 KD and control CD8α^+ cDC1 DCs. The eggs were counted until D18 post-infection (n = 8).

(B) Bar graph showing the intestinal worm counts from activated NCoR1 KD and control cDC1 DC-treated C57BL/6J mice 15 days post-infection (n = 5).

(C) Scatterplot showing the increased effector CD25$^+$FoxP3$^+$ Treg population in MLN of CpG-pulsed NCoR1 KD DC-treated mice compared with control cell-treated animals.

(D) Line graph demonstrating the egg loads in the feces of *H. polygyrus*-infected NCoR1$^{DC-/-}$ and WT C57BL/6J mice at different days post-helminth infection after CpG treatment. The eggs were counted until D17 of infection, and then animals were dissected for intestinal worm counting and T cell profiling from MLNs (n = 5).

(E) Bar plot showing the helminth worm counts from the intestines of CpG-treated NCoR1$^{DC-/-}$ and control C57BL/6J mice on D17 post infection (n = 5).

(F) Bar graph depicting the effector CD25$^+$FoxP3$^+$ Treg cells in the MLNs of CpG-treated NCoR1$^{DC-/-}$ and WT mice 17 days post-helminth infection (n = 5).

(G) Line graph demonstrating the paw inflammation in *L. major*-infected NCoR1$^{DC-/-}$ and WT mice before and after CpG treatment. The CpG treatment was given on D18 after infection. Five animals were used in each group.

(H) Bar plot showing the increase in percentage positive FoxP3 Th cells in draining lymph nodes of NCoR1$^{DC-/-}$ and WT mice at D24 after infection. Five mice were used in each group.

p values are calculated using two-tailed unpaired Student's t test; error bars represent SEM. *p $\leq$ 0.05, **p $\leq$ 0.01. See also Figure S5.

with ChIP-seq data revealed 658 up- and 224 downregulated genes as direct targets of NCoR1 upon CpG activation (Figure 5A, Table S2). The numbers of NCoR1 directly bound and upregulated genes were much higher than the downregulated genes, confirming NCoR1's role as a global transcriptional co-repressor.

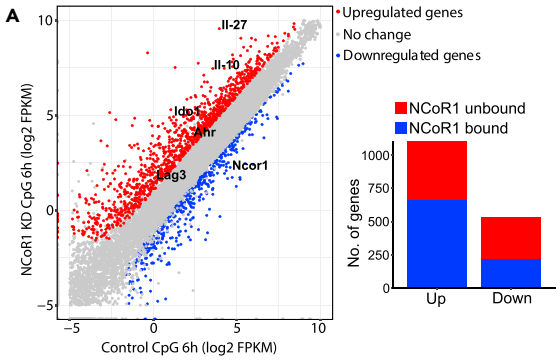

B

S.No.	Enriched Biological Pathways	p-value
1.	IL-10 signaling pathway	4.949E-07
2.	Signal transduction: Erk Interactions: Inhibition of Erk	4.972E-06
3.	Ovarian cancer (main signaling cascades)	6.946E-06
4.	Rheumatoid arthritis (general schema)	7.569E-06
5.	Modulation of tumor response to cytotoxic T cells	7.569E-06
6.	Treg mediated modulation of APC functions	7.900E-06

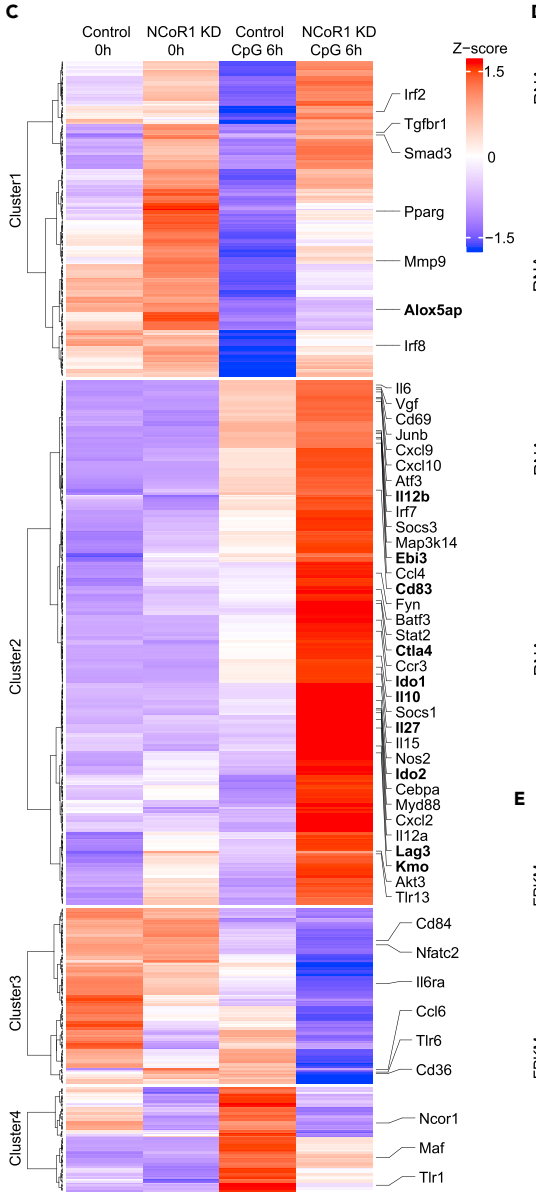

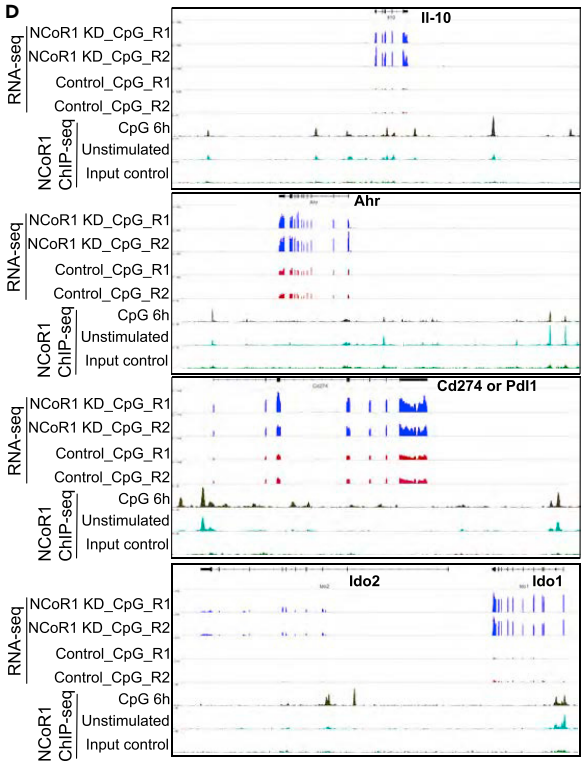

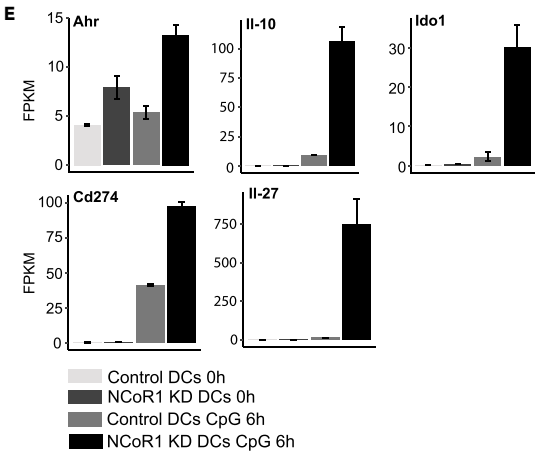

Figure 5. Global Profiling of NCoR1 in cDC1 DC Line Depicts Its Direct Control on DC Tolerance

(A) Scatterplot demonstrating the global RNA-seq data of NCoR1 KD and control CD8α$^+$ cDC1 DC line after 6-h CpG challenge. Red and blue dots indicate the significantly up- and downregulated genes, respectively. Genes of interest are marked in bold. The inset bar graph shows the number of genes directly or indirectly controlled by NCoR1 (n = 2), see also Table S2.

(B) Top biological pathways significantly enriched for the list of direct target genes identified from RNA-seq analysis of 6 h CpG-activated NCoR1 KD DCs. See also Table S4.

(C) Heatmap depicting the clusters observed for the list of genes directly regulated by NCoR1 at 0 h and 6 h after CpG challenge. Important DC immune tolerance genes regulated by NCoR1 are marked in bold. See also Tables S2 and S3.

(D) IGV snapshots showing the NCoR1 binding and RNA-seq tag density observed at *Il-10, Ahr, Pdl1,* and *Ido2* tolerogenic genes.

(E) FPKM (fragment counts/kb/million reads) plots demonstrating the levels of transcript expression for important DC tolerogenicgenes identified to be directly regulated by NCoR1 in CD8α$^+$ cDC1 DCs. See also Table S2.

Pathway enrichment analysis for NCoR1 direct target genes in CpG-activated DCs showed significant enrichment of IL-10 signaling (p value $\leq 10^{-7}$) and Tregs mediated modulation of APC functions (p value $\leq 10^{-6}$) (Figure 5B, Table S4). In contrast, NCoR1-unbound and NCoR1-regulated genes showed pathway enrichments like "Immune response IFN-alpha/beta signaling via MAPKs" and "Cytoskeleton remodeling TGF and WNT and cytoskeletal remodeling" (Table S5). Next, we examined the expression patterns of NCoR1 direct target genes that are differentially regulated in CpG-activated NCoR1 KD cDC1 DCs. Interestingly, cluster 2 revealed a wide variety of tolerogenic genes such as *Lag3, Kmo, Vdr, Cd83,* and *Tgfbr1* along with *Ctla4, Ido1, Ido2, Il-10, Pdl1, and Il-27* (Schinnerling et al., 2015) (Figure 5C, Table S2). integrative genomics viewer (IGV) snapshots and FPKM (fragment counts/kb/million reads) plots from RNA-seq data showed that these genes are highly upregulated after CpG activation in NCoR1-depleted DCs (Figures 5D and 5E). This global analysis further confirmed our *in vitro* and *in vivo* observations that NCoR1 KD cDCs develop strong tolerogenic behavior upon activation.

NCoR1 Strongly Represses the PU.1-Bound Enhancers on Tolerogenic Genes

To identify the molecular mechanism underlying NCoR1-mediated DC tolerance, we have performed an integrative genomic analysis. Our *de novo* motif prediction within NCoR1 ChIP-seq peaks identified PU.1 as highly enriched motifs (55%–60% with p value $\leq 10^{-3}$) in both unstimulated and CpG-challenged conditions (Figures 6A and 6B). Furthermore, RUNX1, BATF, and IRF: BATF motifs were enriched in unstimulated DCs, whereas RUNX1, FRA1, NF-κB, ATF7, and PU.1: IRF motifs were enriched in CpG condition (Figures 6A and 6B). To substantiate our motif predictions, we overlapped NCoR1 binding in cDC1 DC line with publically available TF ChIP-seq data from primary bone marrow-derived dendritic cells (BMDCs) (Garber et al., 2012). We found strong overlap of NCoR1 with PU.1 (50%–55%), NF-–kB (35%–38%), IRF1 (20%–25%), IRF4 (19%–23%), Junb (18%–22%), and the active enhancer mark H3K27ac (60%–65%). Moreover, we performed ChIP-seq and ChIP-qPCR for PU.1 in cDC1 DC line to validate our predictions. We found a strong overlap of PU.1 ($\geq$60%) with NCoR1 peaks, confirming it to be the most putative NCoR1-recruiting factor in DCs (Figures 6C, S6B, and S6C).

To identify the mechanistic control of gene regulation by NCoR1, we did SeqMINER (Ye et al., 2011) clustering to identify the regulatory regions differentially bound by NCoR1 in CpG-activated cDCs compared with unstimulated conditions (Figure S6B). Two of these genomic clusters (clusters I-II) showed increased NCoR1 binding, whereas clusters III-XI showed similar enrichment after activation (Figures 6D and S7A). Interestingly, these regions were annotated to 214 genes that were significantly upregulated in NCoR1 KD DCs upon CpG activation, which includes major tolerogenic genes *Il-10, Pdl1, Ido2, Vdr,* and *Cd83* (Table S6). The cluster I-II genomic regions were also enriched for TFs PU.1, IRF1, IRF4, Junb, and H3K27ac marks, whereas RelA and RelB were enriched only after activation (Figure S6B). Thus, these regulatory regions appear to be the hotspots where several of these activating TFs appear to form complexes.

Moreover, to identify if enhancers at tolerogenic genes are strongly repressed by NCoR1 after CpG challenge, we ran the super-enhancer discovery program to rank PU.1- and NCoR1-bound signals (Table S7). We found that PU.1 super-enhancers on tolerance-inducing genes like *Il-10, Pdl1, Cd83, Ctla4,* and *Tgfβr1* were strongly repressed by NCoR1 after CpG activation (Figures 6E–6G). Our ChIP-qPCR analysis further confirmed the enrichment of PU.1 at these NCoR1-bound genomic regions (Figure S7B). This suggested that NCoR1 masks the PU.1-bound enhancers after DC activation to prevent induction of the major tolerogenic genes. We performed RNA Pol-II ChIP-seq and ChIP-qPCR in control and NCoR1 KD cDC line before and after CpG activation to estimate the changes in transcription rate of differentially regulated genes

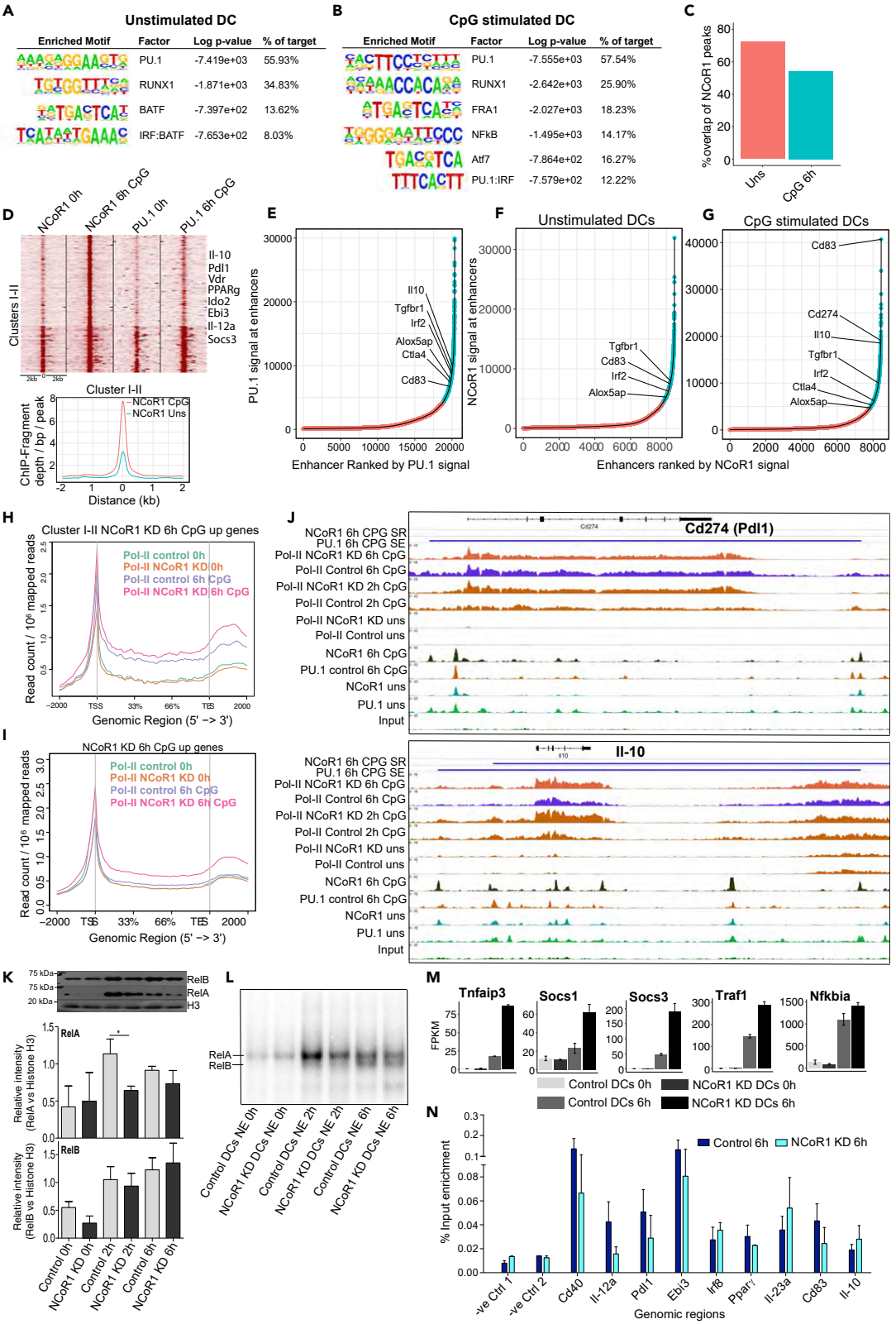
A
Unstimulated DC
Enriched Motif
Factor
Log p-value
% of target
PU.1 -7.419e+03 55.93%
RUNX1 -1.871e+03 34.83%
BATF -7.397e+02 13.62%
IRF:BATF -7.653e+02 8.03%
B
CpG stimulated DC
Enriched Motif
Factor
Log p-value
% of target
PU.1 -7.555e+03 57.54%
RUNX1 -2.642e+03 25.90%
FRA1 -2.027e+03 18.23%
NFkB -1.495e+03 14.17%
Atf7 -7.864e+02 16.27%
PU.1:IRF -7.579e+02 12.22%
C
% overlap of NCoR1 peaks
Uns
CpG 6h
D
NCoR1 0h
NCoR1 6h CpG
PU.1 0h
PU.1 6h CpG
Clusters I-II
Il-10
Pdl1
Vdr
PPARg
Ido2
Ebi3
Il-12a
Socs3
Cluster I-II
NCoR1 CpG
NCoR1 Uns
ChIP-Fragment depth / bp / peak
Distance (kb)
E
PU.1 signal at enhancers
Il10
Tgfbr1
Irf2
Alox5ap
Ctla4
Cd83
Enhancer Ranked by PU.1 signal
F
Unstimulated DCs
NCoR1 signal at enhancers
Tgfbr1
Cd83
Irf2
Alox5ap
Enhancers ranked by NCoR1 signal
G
CpG stimulated DCs
Cd83
Cd274
Il10
Tgfbr1
Irf2
Ctla4
Alox5ap
H
Cluster I-II NCoR1 KD 6h CpG up genes
Pol-II control 0h
Pol-II NCoR1 KD 0h
Pol-II control 6h CpG
Pol-II NCoR1 KD 6h CpG
Read count / 10⁶ mapped reads
Genomic Region (5' –> 3')
I
NCoR1 KD 6h CpG up genes
Pol-II control 0h
Pol-II NCoR1 KD 0h
Pol-II control 6h CpG
Pol-II NCoR1 KD 6h CpG
Read count / 10⁶ mapped reads
Genomic Region (5' –> 3')
J
Cd274 (Pdl1)
NCoR1 6h CPG SR
PU.1 6h CPG SE
Pol-II NCoR1 KD 6h CpG
Pol-II Control 6h CpG
Pol-II NCoR1 KD 2h CpG
Pol-II Control 2h CpG
Pol-II NCoR1 KD uns
Pol-II Control uns
NCoR1 6h CpG
PU.1 control 6h CpG
NCoR1 uns
PU.1 uns
Input
Il-10
NCoR1 6h CPG SR
PU.1 6h CPG SE
Pol-II NCoR1 KD 6h CpG
Pol-II Control 6h CpG
Pol-II NCoR1 KD 2h CpG
Pol-II Control 2h CpG
Pol-II NCoR1 KD uns
Pol-II Control uns
NCoR1 6h CpG
PU.1 control 6h CpG
NCoR1 uns
PU.1 uns
Input
K
RelB
RelA
H3
Relative intensity (RelA vs Histone H3)
Relative intensity (RelB vs Histone H3)
Control 0h
NCoR1 KD 0h
Control 2h
NCoR1 KD 2h
Control 6h
NCoR1 KD 6h
L
RelA
RelB
Control DCs NE 0h
NCoR1 KD DCs NE 0h
Control DCs NE 2h
NCoR1 KD DCs NE 2h
Control DCs NE 6h
NCoR1 KD DCs NE 6h
M
Tnfaip3
Socs1
Socs3
Traf1
Nfkbia
FPKM
Control DCs 0h
NCoR1 KD DCs 0h
Control DCs 6h
NCoR1 KD DCs 6h
N
Control 6h
NCoR1 KD 6h
% Input enrichment
Cd40
Il-12a
Pdl1
Ebi3
Irf8
Pparγ
Il-23a
Cd83
Il-10
Genomic regions

Figure 6. NCoR1 Strongly Represses PU.1-Bound Super-Enhancers Present on Tolerogenic Genes after CpG Activation in CD8α$^+$ cDCs

(A) Top significantly enriched *de novo* predicted DNA motifs of TFs in NCoR1 ChIP-seq peaks of unstimulated CD8α$^+$ cDC1 DC line.

(B) Top significantly enriched DNA motifs of TFs in NCoR1 ChIP-seq peaks of 6-h CpG-stimulated CD8α$^+$ cDC1 DCs.

(C) Bar graph showing the percentage overlap of NCoR1 with PU.1 ChIP-seq peaks before and after 6 h CpG activation.

(D) SeqMINER clustering showing clusters I-II depicting increased NCoR1 binding after CpG activation in cDC1 DC line when compared with unstimulated cells. Corresponding PU.1 ChIP-seq data lanes show its overlap with NCoR1-bound regions. Corresponding density plot shows the differential enrichment of reads in CpG compared with unstimulated at clusters I-II genomic regions. See also Table S6.

(E) Distribution of PU.1 ChIP-seq signals across the total PU.1-bound regulatory regions in CpG-activated CD8α$^+$ DCs. Bound regions were ranked by the tag counts within the PU.1-enriched peaks to identify the super-enhancer regulatory regions or genes. Tolerogenic genes enriched in the PU.1 super-enhancer regions are marked. See also Table S7.

(F and G) Distribution of NCoR1 ChIP-seq signals across the total NCoR1-bound regulatory regions in unstimulated and CpG-activated CD8α$^+$ DCs. Bound regions were ranked by the tag counts within the NCoR1-enriched peaks to identify the regulatory regions or genes super-repressed by NCoR1. Tolerogenic genes enriched in the NCoR1 super-repressed regions are marked. See also Table S7.

(H) Metagene plot showing the RNA Pol-II enrichment in unstimulated and 6-h CpG-stimulated control and NCoR1 KD DCs within the gene-body regions of the genes that are annotated to NCoR1 bound cluster I-II genomic regions.

(I) Metagene plot depicting the RNA Pol-II enrichment profile in unstimulated and 6 h CpG-stimulated control and NCoR1 KD DCs within the gene-body regions of the genes that are upregulated in 6 h CpG-activated NCoR1 KD DCs in RNA-seq data.

(J) IGV snapshots showing the ChIP-seq enrichments of NCoR1, PU.1, and RNA Pol-II at tolerogenic genes Il-10 and Pdl1 at 0 h and 6 h CpG-stimulated CD8α$^+$ cDC1 DC line. RNA-Pol-II enrichment in CpG-activated control and NCoR1 KD DCs demonstrate the real-time transcription of these representative tolerogenic genes. The horizontal bars above the plot show the PU.1-bound super-enhancer (SE) regions that are strongly repressed (SR) by NCoR1 after CpG activation.

(K) Representative western blot picture for NF-κB subunits RelA and RelB depicting their nuclear translocation at 0 h, 2 h, and 6 h after CpG activation in control and NCoR1 KD CD8α$^+$ cDC1 line. Corresponding densitometric analysis bar plots shows the relative intensity of RelA and RelB from four biological replicates (n = 4).

(L) Electrophoretic mobility shift assay (EMSA) demonstrating the binding activity of RelA and RelB at 0 h, 2 h, and 6 h after CpG activation. RelA and RelB bands are indicated by the marks.

(M) Fragment counts/kb/million read counts plots from control and NCoR1 KD RNA-seq data showing the differential expression of NF-κB negative regulators of NF-κB canonical signaling.

(N) RelA ChIP-qPCR depicting the enrichment of RelA at 10 randomly selected genomic regions when compared with negative control genomic regions. p values are calculated using two-tailed paired Student's t test; fold change error is depicted as SEM. *$p \leq 0.05$. See also Figures S6 and S7.

(Figure S7C). We observed profoundly increased gene body RNA Pol-II tag counts for the cluster I-II annotated genes that are upregulated in NCoR1-depleted cDCs (Figures 6H–6J). The downregulated genes showed a decreased Pol-II tag density (Figures S7C and S7D). Representative IGV snapshots depicted the normalized ChIP-seq and RNA-seq tag counts at major tolerogenic genes *Il-10* and *Pdl1* (Figure 6J).

Collectively, these results demonstrated that NCoR1 directly represses the tolerogenic enhancers after DC activation. Hence upon NCoR1 depletion, these genes are derepressed leading to their enhanced transcription and concomitant mRNA expression after DC activation. This NCoR1-mediated repression of the tolerogenic program appears to be a very important event to prevent the cDCs from going into tolerogenic modality under the strong inflammatory stimulus.

NCoR1 Depletion Perturbs NF-κB Activity on Tolerogenic Genes

We found a significant enrichment of NF-κB DNA motif in NCoR1-bound regions, and a fine balance of NF-κB activity controlling the immunogenic versus regulatory phenotype in DCs has been widely reported (Dohler et al., 2017; Thomas, 2013; Vendelova et al., 2018). Therefore, two mechanisms could be suggested: (1) NCoR1 directly represses PU.1-regulated tolerogenic genes and (2) it directly represses inhibitors of RelA (NF-κB), which provides for immunogenic functions. Therefore, we probed NF-κB nuclear translocation (RelA and RelB) and binding activity in NCoR1 KD and control cDC1 DCs before and after CpG activation. We found significantly inhibited RelA translocation and activity in NCoR1-depleted DCs at 2 h after activation, whereas RelB activity was unaffected (Figures 6K and 6L). We found increased RelA nuclear localization and binding at 2 h when compared with 6 h, whereas RelB comes up at 6 h after CpG activation. Interestingly, NCoR1 had little, if any, impact on RelB activity, which is known for immune tolerance in DCs. In addition, we also observed significantly increased expression of negative regulators of NF-κB signaling, i.e., *Tnfaip3*, Nfkbia, and *Traf1* along with cytokine-signaling regulators *Socs1* and *Socs3* in NCoR1 KD DCs (Figure 6M). RelA ChIP-qPCR further confirmed an overall decreased RelA enrichment on selected tolerogenic/immunogenic genes except Il-10 and Il-23a in activated NCoR1-depleted DCs (Figure 6N). This indicated toward a role of NCoR1 in perturbing NF-κB activity to fine-tune DCs immunogenic versus tolerogenic state.

DISCUSSION

DCs link innate to adaptive immunity and regulate a fine balance of inflammatory and tolerogenic responses to prevent immune pathology. Although the signaling pathways underlying immunogenic and tolerogenic program are explored, the mechanisms underlying fine control of this balance in DCs is of paramount interest for therapeutic approaches and are largely unknown. Using *in vitro*, *ex vivo*, and *in vivo* models, we revealed that NCoR1 is a master repressor of the tolerogenic program in cDC1 DCs and its depletion renders DCs tolerogenic, irrespective of activation by any strong TLR ligand or microbe. NCoR1-depleted DCs have strong potential to polarize Th cells into Tregs *ex vivo* and *in vivo* with a concomitant increase in disease phenotype. Moreover, we demonstrated using integrative genomic analyses that NCoR1 strongly represses tolerogenic genes and its KD modulates NF-κB activity in activated DCs that could shift immunogenic program toward tolerance.

A number of reports suggested that treatment of DCs with a variety of strong NR ligands such as vitamin-D and dexamethasone induces DC tolerance by suppressing their activation along with an increased IL-10 production (Anderson et al., 2017). NRs are well known to control their target genes by switching from co-repressor to co-activator complexes upon stimulation (McKenna and O'Malley, 2002; Mouchiroud et al., 2014). Recently, NCoR1 co-repressor has been reported to interact with non-NR TFs such as NF-κB and AP1 that are crucial for DC function (Barish et al., 2012; Huang et al., 2009; Li et al., 2013). Activation signals remove NCoR1 from co-repressor complex through recruitment of activating TFs like NF-κB or through complex destabilization by kinases such as p38 and pErk (Ghisletti et al., 2009). In DCs CpG stimulation activates canonical NF-κB signaling along with phosphorylation of p38 and Erk kinases (O'Neill et al., 2013; Yu et al., 2004). Activation of Erk kinase is predominantly reported to induce IL-10 expression, whereas p38 largely induces inflammatory cytokines like IL-12 (Saraiva and O'Garra, 2010; Yu et al., 2004). We found a profoundly increased pErk activity and concomitantly increased IL-10 levels in activated NCoR1 KD DCs. At the same time PDL1, IL-27, and IDO1 genes were upregulated, which are also reported to induce strong tolerogenic responses (Raker et al., 2015; Shiokawa et al., 2009; Sumpter and Thomson, 2011; Yoo and Ha, 2016). The IL-10 cytokine further induces *Pdl1* through STAT3 signaling (Wolfle et al., 2011). The expression of major tolerogenic genes like Ido1, Pdl1, and Il-10 are also induced by IL-27 cytokine, an IL-12 family member cytokine through STAT1 and STAT3 signaling (Carbotti et al., 2015; Murugaiyan et al., 2009). Both these STATs were increased in NCoR1 KD DCs (Carbotti et al., 2015), which are known to induce regulatory Tr1 cells by inhibiting Th17 cell development (Kushwah and Hu, 2011). The increased IL-2 could also enhance the secretion of IL-27-induced IL-10 (Murugaiyan et al., 2009). Studies suggest that STAT3 is also phosphorylated via both IL-6 and IL-10 signaling in immune cells (Niemand et al., 2003). It is unlikely that increased IL-6 is responsible for this STAT3 activation in NCoR1 KD cells as the *IL-6rα* expression was significantly decreased after CpG stimulation. There is a concomitant increase in *Socs3* as well, which strongly inhibits STAT3 phosphorylation leaving open the IL-10 signaling pathway (Ahmed and Ivashkiv, 2000). Socs2 and Socs3 are also reported to suppress uncontrolled inflammatory cytokine expression and were highly elevated in tolerogenic-state mature DCs (Connor et al., 2017; Yoshimura et al., 2005).

Contrary to the reported suppression of IL-12 by enhanced IL-10 signaling in DCs (Ma et al., 2015), we noticed a marginal increase of IL-12 in NCoR1 KD DCs when compared with the robust increase of IL-10 production. Last but not the least, IL-12p40 homo-dimers are inhibitory and IL-12p70 is not significantly up-regulated in NCoR1 KD DCs. Type-I IFN signaling is also suggested to stimulate IL-10 and suppress IL-12 and IL-23 cytokines in DCs (Yen et al., 2015). Interestingly, we found *Ifnβ1* and its signaling intermediate *Stat2* significantly increased in CpG-stimulated NCoR1 KD DCs. IFNβ1 is also known to represses IL-12 expression (Zhao et al., 2015).

Some of the surface markers and secreted factors that showed a marginal increase after NCoR1 KD are often considered inflammatory. Nevertheless, co-stimulation and antigen presentation by MHC class-II are required for Treg generation (Price et al., 2015). Therefore, an increase of co-stimulatory molecules can also contribute to Treg differentiation. As Tregs express CD25 (IL-2Rα), increased IL-2 secreted by NCoR1 KD DCs could induce Treg proliferation and clonal expansion and further contribute to tolerogenicity. In RNA-seq, we find upregulation of IL-12p35 and this molecule has inflammatory (IL-12p70) as well as anti-inflammatory/tolerogenic properties (IL-35 composed of IL-12p35 and EBI3) (Collison et al., 2010).

Furthermore, we characterized the direct and indirect target genes of NCoR1 for mechanistic insight. We found a strong overlap of PU.1 binding with NCoR1, suggesting it as the most putative TF-tethering NCoR1 in DCs. Integrative genomics demonstrated that NCoR1 masks the PU.1-bound super-enhancers at the major

tolerogenic genes including *Il-10, Cd83, Ctla4,* and *Pdl1*. Therefore, upon NCoR1 depletion these genes are derepressed leading to enhanced transcription as evident by increased gene body RNA Pol-II counts after activation. We also observed a significant enrichment of NF-κB at NCoR1 peaks in CpG-activated condition, which suggested involvement of NF-κB TF in NCoR1-mediated effects. Recent reports also indicated that perturbations in the activity of different NF-κB subunits like RelA and RelB modulate DCs' inflammatory versus tolerogenic phenotype (Azukizawa et al., 2011). We identified that RelA-binding activity was profoundly reduced after activation, whereas RelB was unaffected. In addition, NCoR1 directly represses negative regulators of canonical NF-κB signaling such as Tnfaip3 (A20), Traf1, and Pias1, which are well reported to repress inflammatory responses by inhibiting RelA activity (Kool et al., 2011; Liu et al., 2005a; Sen and Smale, 2010; Vereecke et al., 2009). We also noticed increased RelB translocation and activity from 2 to 6 h after CpG activation in CD8α^+ cDCs, whereas the RelA activity was reduced. It would be further interesting to characterize how this switch of NF-κB activity regulates DC responses. In addition, we showed that increased NCoR1 biding after CpG activation overlaps with binding of other activating TFs. Therefore, it is highly probable that other activating TFs may also bind at these tolerogenic enhancers after NCoR1 depletion. Treatment with live bacteria showed even more pronounced tolerogenic effects compared with CpG challenge, which suggests that multiple strong stimulations further enhance tolerogenicity in NCoR1 KD DCs. Altogether, our integrative genomic analysis identified NCoR1 as a master regulator of the tolerogenic program in DCs.

Limitations of the Study

In this study we have majorly used cDC1 mutuDC line and validated the findings *ex vivo and in vivo* using primary DCs. It is important to mention that from a single WT C57BL/6 mice one can get nearly 100,000 cDC1 DCs in good condition from splenocytes, using magnetic bead-based kits. Therefore, using primary DCs is a major limitation for high-throughput genomic analysis such as ChIP-seq and bulk RNA-seq that we reported here.

SUPPLEMENTAL INFORMATION

Supplemental Information can be found online at https://doi.org/10.1016/j.isci.2019.08.024.

METHODS

All methods can be found in the accompanying Transparent Methods supplemental file.

ACKNOWLEDGMENTS

We thank Johan Auwerx for providing the NCoR1$^{fl/fl}$ mice, Genotypic technology for NGS, Fabienne Tacchini-Cottier, Ivo Regli, and Marianna Koga for helping in the parasite experiments and Matteo Pigni for providing the CD11b cDC line. Nicola Harris lab at EPFL, Lausanne, provided the helminth larvae. We thank Christine Lavanchy, Viplov K. Biswas and Vanessa Mack for their technical help. Ton Rolink provided the FLT3L transgenic mice. We thank Bart Deplancke, Marjan Biocanin, and Punit Prasad for constructive comments to edit the manuscript and Girdhari Lal of NCCS Pune, India for suggestions during revision. A.A. is supported by DBT-JRF. S.S. is supported by ILS fellowship. G.P.M. is supported by DBT BINC fellowship and DST-SNSF grant. Grant funds from DST-SNSF (DST/INT/SWISS/SNSF/P-47/2015), DBT-India Ramalingaswami fellowship, SERB-India (EMR/2016/000717), DBT-India (BT/PR15908/MED/12/725/2016), (HAO_SNF-Switzerland 310030_132492) supported this study; ILS provided intramural support and infrastructure.

AUTHOR CONTRIBUTIONS

Conceptualization, A.A., M.S., S.S., S.K.R., and H.A-O.; Methodology, A.A., S.S., M.S., D.G., U.A.S., and B.G.; Investigation, A.A., M.S., S.S., S.B., H.A-O., and S.K.R.; Writing – Original Draft, A.A., M.S., H.A-O., B.G., and S.K.R.; Data Curation, G.P.M. and S.K.R.; Formal Analysis, G.P.M. and S.M.W.; Supervision, S.K.R. and H.A-O.; Visualization, A.A., S.S., G.P.M., and M.S.; Funding Acquisition, S.K.R. and H.A-O.

DECLARATION OF INTERESTS

The authors declare no competing interests.

Received: February 27, 2019
Revised: June 19, 2019
Accepted: August 13, 2019
Published: September 27, 2019

REFERENCES

Agrawal, S., Ganguly, S., Tran, A., Sundaram, P., and Agrawal, A. (2016). Retinoic acid treated human dendritic cells induce T regulatory cells via the expression of CD141 and GARP which is impaired with age. Aging (Albany NY) *8*, 1223–1235.

Ahmed, S.T., and Ivashkiv, L.B. (2000). Inhibition of IL-6 and IL-10 signaling and Stat activation by inflammatory and stress pathways. J. Immunol. *165*, 5227–5237.

Anderson, A.E., Swan, D.J., Wong, O.Y., Buck, M., Eltherington, O., Harry, R.A., Patterson, A.M., Pratt, A.G., Reynolds, G., Doran, J.P., et al. (2017). Tolerogenic dendritic cells generated with dexamethasone and vitamin D3 regulate rheumatoid arthritis CD4+ T cells partly via transforming growth factor-beta1. Clin. Exp. Immunol. *187*, 113–123.

Ashok, D., Schuster, S., Ronet, C., Rosa, M., Mack, V., Lavanchy, C., Marraco, S.F., Fasel, N., Murphy, K.M., Tacchini-Cottier, F., et al. (2014). Cross-presenting dendritic cells are required for control of Leishmania major infection. Eur. J. Immunol. *44*, 1422–1432.

Azukizawa, H., Dohler, A., Kanazawa, N., Nayak, A., Lipp, M., Malissen, B., Autenrieth, I., Katayama, I., Riemann, M., Weih, F., et al. (2011). Steady state migratory RelB+ langerin+ dermal dendritic cells mediate peripheral induction of antigen-specific CD4+ CD25+ Foxp3+ regulatory T cells. Eur. J. Immunol. *41*, 1420–1434.

Baerenwaldt, A., von Burg, N., Kreuzaler, M., Sitte, S., Horvath, E., Peter, A., Voehringer, D., Rolink, A.G., and Finke, D. (2016). Flt3 ligand regulates the development of innate lymphoid cells in fetal and adult mice. J. Immunol. *196*, 2561–2571.

Barish, G.D., Yu, R.T., Karunasiri, M.S., Becerra, D., Kim, J., Tseng, T.W., Tai, L.J., Leblanc, M., Diehl, C., Cerchietti, L., et al. (2012). The Bcl6-SMRT/NCoR cistrome represses inflammation to attenuate atherosclerosis. Cell Metab. *15*, 554–562.

Carbotti, G., Barisione, G., Airoldi, I., Mezzanzanica, D., Bagnoli, M., Ferrero, S., Petretto, A., Fabbi, M., and Ferrini, S. (2015). IL-27 induces the expression of IDO and PD-L1 in human cancer cells. Oncotarget *6*, 43267–43280.

Cohen, R.N., Wondisford, F.E., and Hollenberg, A.N. (1998). Two separate NCoR (nuclear receptor corepressor) interaction domains mediate corepressor action on thyroid hormone response elements. Mol. Endocrinol. *12*, 1567–1581.

Collison, L.W., Chaturvedi, V., Henderson, A.L., Giacomin, P.R., Guy, C., Bankoti, J., Finkelstein, D., Forbes, K., Workman, C.J., Brown, S.A., et al. (2010). IL-35-mediated induction of a potent regulatory T cell population. Nat. Immunol. *11*, 1093–1101.

Connor, L.M., Tang, S.C., Cognard, E., Ochiai, S., Hilligan, K.L., Old, S.I., Pellefigues, C., White, R.F., Patel, D., Smith, A.A., et al. (2017). Th2 responses are primed by skin dendritic cells with distinct transcriptional profiles. J. Exp. Med. *214*, 125–142.

Couper, K.N., Blount, D.G., and Riley, E.M. (2008). IL-10: the master regulator of immunity to infection. J. Immunol. *180*, 5771–5777.

Dohler, A., Schneider, T., Eckert, I., Ribechini, E., Andreas, N., Riemann, M., Reizis, B., Weih, F., and Lutz, M.B. (2017). RelB(+) steady-state migratory dendritic cells control the peripheral pool of the natural Foxp3(+) regulatory T cells. Front Immunol. *8*, 726.

Farias, A.S., Spagnol, G.S., Bordeaux-Rego, P., Oliveira, C.O., Fontana, A.G., de Paula, R.F., Santos, M.P., Pradella, F., Moraes, A.S., Oliveira, E.C., et al. (2013). Vitamin D3 induces IDO+ tolerogenic DCs and enhances Treg, reducing the severity of EAE. CNS Neurosci. Ther. *19*, 269–277.

Filbey, K.J., Grainger, J.R., Smith, K.A., Boon, L., van Rooijen, N., Harcus, Y., Jenkins, S., Hewitson, J.P., and Maizels, R.M. (2014). Innate and adaptive type 2 immune cell responses in genetically controlled resistance to intestinal helminth infection. Immunol. Cell Biol. *92*, 436–448.

Fuertes Marraco, S.A., Grosjean, F., Duval, A., Rosa, M., Lavanchy, C., Ashok, D., Haller, S., Otten, L.A., Steiner, Q.G., Descombes, P., et al. (2012). Novel murine dendritic cell lines: a powerful auxiliary tool for dendritic cell research. Front Immunol. *3*, 331.

Garber, M., Yosef, N., Goren, A., Raychowdhury, R., Thielke, A., Guttman, M., Robinson, J., Minie, B., Chevrier, N., Itzhaki, Z., et al. (2012). A high-throughput chromatin immunoprecipitation approach reveals principles of dynamic gene regulation in mammals. Mol. Cell *47*, 810–822.

Ghisletti, S., Huang, W., Jepsen, K., Benner, C., Hardiman, G., Rosenfeld, M.G., and Glass, C.K. (2009). Cooperative NCoR/SMRT interactions establish a corepressor-based strategy for integration of inflammatory and anti-inflammatory signaling pathways. Genes Dev. *23*, 681–693.

Hochweller, K., Wabnitz, G.H., Samstag, Y., Suffner, J., Hammerling, G.J., and Garbi, N. (2010). Dendritic cells control T cell tonic signaling required for responsiveness to foreign antigen. Proc. Natl. Acad. Sci. U S A *107*, 5931–5936.

Huang, W., Ghisletti, S., Perissi, V., Rosenfeld, M.G., and Glass, C.K. (2009). Transcriptional integration of TLR2 and TLR4 signaling at the NCoR derepression checkpoint. Mol. Cell *35*, 48–57.

Kaiko, G.E., Horvat, J.C., Beagley, K.W., and Hansbro, P.M. (2008). Immunological decision-making: how does the immune system decide to mount a helper T-cell response? Immunology *123*, 326–338.

Kapsenberg, M.L. (2003). Dendritic-cell control of pathogen-driven T-cell polarization. Nat. Rev. Immunol. *3*, 984–993.

Kawasaki, T., and Kawai, T. (2014). Toll-like receptor signaling pathways. Front Immunol. *5*, 461.

Kool, M., van Loo, G., Waelput, W., De Prijck, S., Muskens, F., Sze, M., van Praet, J., Branco-Madeira, F., Janssens, S., Reizis, B., et al. (2011). The ubiquitin-editing protein A20 prevents dendritic cell activation, recognition of apoptotic cells, and systemic autoimmunity. Immunity *35*, 82–96.

Kowalczyk, A., D'Souza, C.A., and Zhang, L. (2014). Cell-extrinsic CTLA4-mediated regulation of dendritic cell maturation depends on STAT3. Eur. J. Immunol. *44*, 1143–1155.

Kushwah, R., and Hu, J. (2011). Role of dendritic cells in the induction of regulatory T cells. Cell Biosci. *1*, 20.

Li, P., Spann, N.J., Kaikkonen, M.U., Lu, M., Oh, D.Y., Fox, J.N., Bandyopadhyay, G., Talukdar, S., Xu, J., Lagakos, W.S., et al. (2013). NCoR repression of LXRs restricts macrophage biosynthesis of insulin-sensitizing omega 3 fatty acids. Cell *155*, 200–214.

Liu, B., Yang, R., Wong, K.A., Getman, C., Stein, N., Teitell, M.A., Cheng, G., Wu, H., and Shuai, K. (2005a). Negative regulation of NF-kappaB signaling by PIAS1. Mol. Cell. Biol. *25*, 1113–1123.

Liu, J., Cao, S., Kim, S., Chung, E.Y., Homma, Y., Guan, X., Jimenez, V., and Ma, X. (2005b). Interleukin-12: an update on its immunological activities, signaling and regulation of gene expression. Curr. Immunol. Rev. *1*, 119–137.

Ma, X., Yan, W., Zheng, H., Du, Q., Zhang, L., Ban, Y., Li, N., and Wei, F. (2015). Regulation of IL-10 and IL-12 production and function in macrophages and dendritic cells. F1000Res *4*, 1465.

MacDonald, A.S., and Maizels, R.M. (2008). Alarming dendritic cells for Th2 induction. J. Exp. Med. *205*, 13–17.

Matsushima, H., Yamada, N., Matsue, H., and Shimada, S. (2004). TLR3-, TLR7-, and TLR9-mediated production of proinflammatory cytokines and chemokines from murine connective tissue type skin-derived mast cells but not from bone marrow-derived mast cells. J. Immunol. *173*, 531–541.

McKenna, N.J., and O'Malley, B.W. (2002). Combinatorial control of gene expression by nuclear receptors and coregulators. Cell *108*, 465–474.

Mellor, A.L., and Munn, D.H. (2004). IDO expression by dendritic cells: tolerance and tryptophan catabolism. Nat. Rev. Immunol. *4*, 762–774.

Moreau, A., Alliot-Licht, B., Cuturi, M.C., and Blancho, G. (2017). Tolerogenic dendritic cell therapy in organ transplantation. Transpl. Int. *30*, 754–764.

Mottis, A., Mouchiroud, L., and Auwerx, J. (2013). Emerging roles of the corepressors NCoR1 and SMRT in homeostasis. Genes Dev. *27*, 819–835.

Mouchiroud, L., Eichner, L.J., Shaw, R.J., and Auwerx, J. (2014). Transcriptional coregulators: fine-tuning metabolism. Cell Metab. *20*, 26–40.

Murugaiyan, G., Mittal, A., Lopez-Diego, R., Maier, L.M., Anderson, D.E., and Weiner, H.L. (2009). IL-27 is a key regulator of IL-10 and IL-17

production by human CD4+ T cells. J. Immunol. *183*, 2435–2443.

Ng, S.S., Chang, T.H., Tailor, P., Ozato, K., and Kino, T. (2011). Virus-induced differential expression of nuclear receptors and coregulators in dendritic cells: implication to interferon production. FEBS Lett. *585*, 1331–1337.

Niemand, C., Nimmesgern, A., Haan, S., Fischer, P., Schaper, F., Rossaint, R., Heinrich, P.C., and Muller-Newen, G. (2003). Activation of STAT3 by IL-6 and IL-10 in primary human macrophages is differentially modulated by suppressor of cytokine signaling 3. J. Immunol. *170*, 3263–3272.

O'Neill, L.A., Golenbock, D., and Bowie, A.G. (2013). The history of Toll-like receptors - redefining innate immunity. Nat. Rev. Immunol. *13*, 453–460.

Perissi, V., Scafoglio, C., Zhang, J., Ohgi, K.A., Rose, D.W., Glass, C.K., and Rosenfeld, M.G. (2008). TBL1 and TBLR1 phosphorylation on regulated gene promoters overcomes dual CtBP and NCoR/SMRT transcriptional repression checkpoints. Mol. Cell *29*, 755–766.

Pigni, M., Ashok, D., Stevanin, M., and Acha-Orbea, H. (2018). Establishment and characterization of a functionally competent type 2 conventional dendritic cell line. Front Immunol. *9*, 1912.

Price, J.G., Idoyaga, J., Salmon, H., Hogstad, B., Bigarella, C.L., Ghaffari, S., Leboeuf, M., and Merad, M. (2015). CDKN1A regulates Langerhans cell survival and promotes Treg cell generation upon exposure to ionizing irradiation. Nat. Immunol. *16*, 1060–1068.

Raghav, S.K., Waszak, S.M., Krier, I., Gubelmann, C., Isakova, A., Mikkelsen, T.S., and Deplancke, B. (2012). Integrative genomics identifies the corepressor SMRT as a gatekeeper of adipogenesis through the transcription factors C/EBPbeta and KAISO. Mol. Cell *46*, 335–350.

Raker, V.K., Domogalla, M.P., and Steinbrink, K. (2015). Tolerogenic dendritic cells for regulatory T cell induction in man. Front Immunol. *6*, 569.

Reizis, B. (2011). Intracellular pathogens and CD8(+) dendritic cells: dangerous liaisons. Immunity *35*, 153–155.

Saraiva, M., and O'Garra, A. (2010). The regulation of IL-10 production by immune cells. Nat. Rev. Immunol. *10*, 170–181.

Schinnerling, K., Garcia-Gonzalez, P., and Aguillon, J.C. (2015). Gene expression profiling of human monocyte-derived dendritic cells - searching for molecular regulators of tolerogenicity. Front Immunol. *6*, 528.

Schnorrer, P., Behrens, G.M., Wilson, N.S., Pooley, J.L., Smith, C.M., El-Sukkari, D., Davey, G., Kupresanin, F., Li, M., Maraskovsky, E., et al. (2006). The dominant role of CD8+ dendritic cells in cross-presentation is not dictated by antigen capture. Proc. Natl. Acad. Sci. U S A *103*, 10729–10734.

Sen, R., and Smale, S.T. (2010). Selectivity of the NF-{kappa}B response. Cold Spring Harb Perspect. Biol. *2*, a000257.

Shih, V.F., Davis-Turak, J., Macal, M., Huang, J.Q., Ponomarenko, J., Kearns, J.D., Yu, T., Fagerlund, R., Asagiri, M., Zuniga, E.I., et al. (2012). Control of RelB during dendritic cell activation integrates canonical and noncanonical NF-kappaB pathways. Nat. Immunol. *13*, 1162–1170.

Shiokawa, A., Tanabe, K., Tsuji, N.M., Sato, R., and Hachimura, S. (2009). IL-10 and IL-27 producing dendritic cells capable of enhancing IL-10 production of T cells are induced in oral tolerance. Immunol. Lett. *125*, 7–14.

Smita, S., Ahad, A., Ghosh, A., Biswas, V.K., Koga, M.M., Gupta, B., Acha-Orbea, H., and Raghav, S.K. (2018). Importance of EMT factor ZEB1 in cDC1 "MutuDC line" mediated induction of Th1 immune response. Front Immunol. *9*, 2604.

Steinman, R.M. (2006). Linking innate to adaptive immunity through dendritic cells. Novartis Found. Symp. *279*, 101–109, discussion 109-113, 216-109.

Sumpter, T.L., and Thomson, A.W. (2011). The STATus of PD-L1 (B7-H1) on tolerogenic APCs. Eur. J. Immunol. *41*, 286–290.

Takeuchi, O., and Akira, S. (2010). Pattern recognition receptors and inflammation. Cell *140*, 805–820.

Taylor, M.D., van der Werf, N., and Maizels, R.M. (2012). T cells in helminth infection: the regulators and the regulated. Trends Immunol. *33*, 181–189.

Thomas, R. (2013). RelB and the aryl hydrocarbon receptor: dendritic cell tolerance at the epithelial interface. Immunol. Cell Biol. *91*, 543–544.

Thompson, P.W., Bayliffe, A.I., Warren, A.P., and Lamb, J.R. (2007). Interleukin-10 is upregulated by nanomolar rosiglitazone treatment of mature dendritic cells and human CD4+ T cells. Cytokine *39*, 184–191.

Tsoumakidou, M., Tousa, S., Semitekolou, M., Panagiotou, P., Panagiotou, A., Morianos, I., Litsiou, E., Trochoutsou, A.I., Konstantinou, M., Potaris, K., et al. (2014). Tolerogenic signaling by pulmonary CD1c+ dendritic cells induces regulatory T cells in patients with chronic obstructive pulmonary disease by IL-27/IL-10/inducible costimulator ligand. J. Allergy Clin. Immunol. *134*, 944–954.e8.

Vendelova, E., Ashour, D., Blank, P., Erhard, F., Saliba, A.E., Kalinke, U., and Lutz, M.B. (2018). Tolerogenic transcriptional signatures of steady-state and pathogen-induced dendritic cells. Front Immunol. *9*, 333.

Vereecke, L., Beyaert, R., and van Loo, G. (2009). The ubiquitin-editing enzyme A20 (TNFAIP3) is a central regulator of immunopathology. Trends Immunol. *30*, 383–391.

Wolfle, S.J., Strebovsky, J., Bartz, H., Sahr, A., Arnold, C., Kaiser, C., Dalpke, A.H., and Heeg, K. (2011). PD-L1 expression on tolerogenic APCs is controlled by STAT-3. Eur. J. Immunol. *41*, 413–424.

Yamamoto, H., Williams, E.G., Mouchiroud, L., Canto, C., Fan, W., Downes, M., Heligon, C., Barish, G.D., Desvergne, B., Evans, R.M., et al. (2011). NCoR1 is a conserved physiological modulator of muscle mass and oxidative function. Cell *147*, 827–839.

Yan, Y., Zhang, G.X., Gran, B., Fallarino, F., Yu, S., Li, H., Cullimore, M.L., Rostami, A., and Xu, H. (2010). IDO upregulates regulatory T cells via tryptophan catabolite and suppresses encephalitogenic T cell responses in experimental autoimmune encephalomyelitis. J. Immunol. *185*, 5953–5961.

Ye, T., Krebs, A.R., Choukrallah, M.A., Keime, C., Plewniak, F., Davidson, I., and Tora, L. (2011). seqMINER: an integrated ChIP-seq data interpretation platform. Nucleic Acids Res. *39*, e35.

Yen, J.H., Kong, W., Hooper, K.M., Emig, F., Rahbari, K.M., Kuo, P.C., Scofield, B.A., and Ganea, D. (2015). Differential effects of IFN-beta on IL-12, IL-23, and IL-10 expression in TLR-stimulated dendritic cells. J. Leukoc. Biol. *98*, 689–702.

Yoo, S., and Ha, S.J. (2016). Generation of tolerogenic dendritic cells and their therapeutic applications. Immune Netw. *16*, 52–60.

Yoshimura, A., Nishinakamura, H., Matsumura, Y., and Hanada, T. (2005). Negative regulation of cytokine signaling and immune responses by SOCS proteins. Arthritis Res. Ther. *7*, 100–110.

Yu, C., Markan, K., Temple, K.A., Deplewski, D., Brady, M.J., and Cohen, R.N. (2005). The nuclear receptor corepressors NCoR and SMRT decrease peroxisome proliferator-activated receptor gamma transcriptional activity and repress 3T3-L1 adipogenesis. J. Biol. Chem. *280*, 13600–13605.

Yu, Q., Kovacs, C., Yue, F.Y., and Ostrowski, M.A. (2004). The role of the p38 mitogen-activated protein kinase, extracellular signal-regulated kinase, and phosphoinositide-3-OH kinase signal transduction pathways in CD40 ligand-induced dendritic cell activation and expansion of virus-specific CD8+ T cell memory responses. J. Immunol. *172*, 6047–6056.

Zhao, G.N., Jiang, D.S., and Li, H. (2015). Interferon regulatory factors: at the crossroads of immunity, metabolism, and disease. Biochim. Biophys. Acta *1852*, 365–378.

ISCI, Volume *19*

Supplemental Information

NCoR1: Putting the Brakes on the Dendritic Cell Immune Tolerance

Abdul Ahad, Mathias Stevanin, Shuchi Smita, Gyan Prakash Mishra, Dheerendra Gupta, Sebastian Waszak, Uday Aditya Sarkar, Soumen Basak, Bhawna Gupta, Hans Acha-Orbea, and Sunil Kumar Raghav

Figure S1: Related to Figure 1

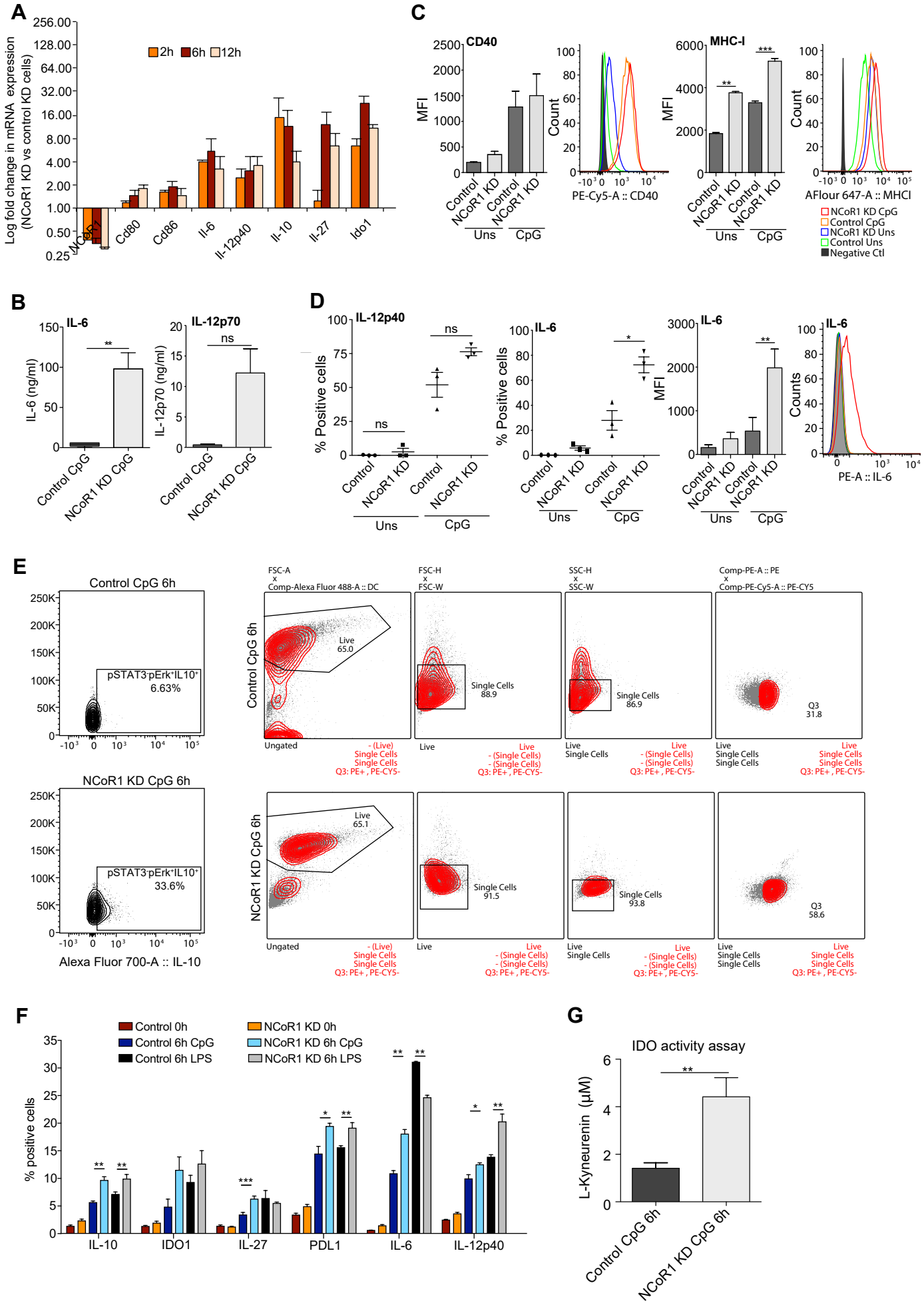

Figure S1. (Related to figure 1) NCoR1 KD cDCs (CD8α^+ and CD11b$^+$ DCs) show tolerogenic behavior after CpG activation *in vitro.*

A. RT-qPCR kinetics showing the transcript levels of selected DC response genes in NCoR1 KD and control cDC1 DC line after 2h, 6h and 12h CpG activation. (n=3)
B. Bio-Plex quantitation of secreted cytokines IL-6 and IL-12p70 in the culture supernatants of 6h CpG activated NCoR1 KD and control CD8α^+ DC. (n=6)
C. Bar plots showing the MFI shifts for co-stimulatory genes CD40 and MHC-I in in NCoR1 KD DCs and control cDC 1 DC line. (n=4) Corresponding histograms depict the representative MFI shifts.
D. Scatter-plots depicting the percentage positive cells for intracellular cytokines IL-6 and IL-12p40 in NCoR1 KD and control CD8α^+ cDC1 DCs before and after CpG stimulation. (n=4) Corresponding histograms depict the representative MFI shifts.
E. Contour-plots showing the percentages of pErk$^+$IL-10$^+$Stat3$^-$ cells in 6h CpG activated NCoR1 KD and control DCs. Gating strategy used to identify pErk$^+$STAT3$^-$IL-10$^+$ DCs in 6h CpG activated control and NCoR1 KD DCs. (n=3)
F. Bar-graph for flow cytometric data demonstrating percentage of positive cells for IL-10, IDO1, IL-27, PDL1, IL-6 and IL-12p40 in unstimulated, 6h CpG or LPS activated NCoR1 KD and control CD11b$^+$ cDC2 DCs. (n=3)
G. IDO activity assay showing the amount of L-Kynurenine produced in the culture supernatant of 6h CpG activated NCoR1 KD and control DCs. (n=3)

p-values are calculated using two tailed paired *t*-test. Error bars represent SEM.
*$\leq$ 0.05, **$\leq$ 0.01, ***$\leq$ 0.001

Figure S2. Related to Figure 1

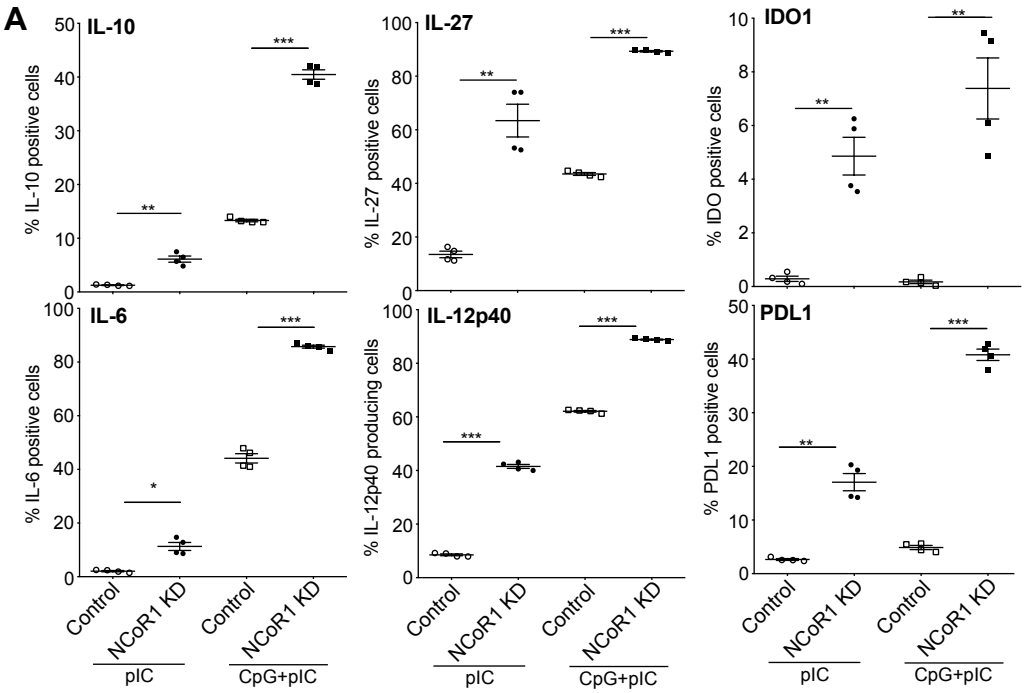

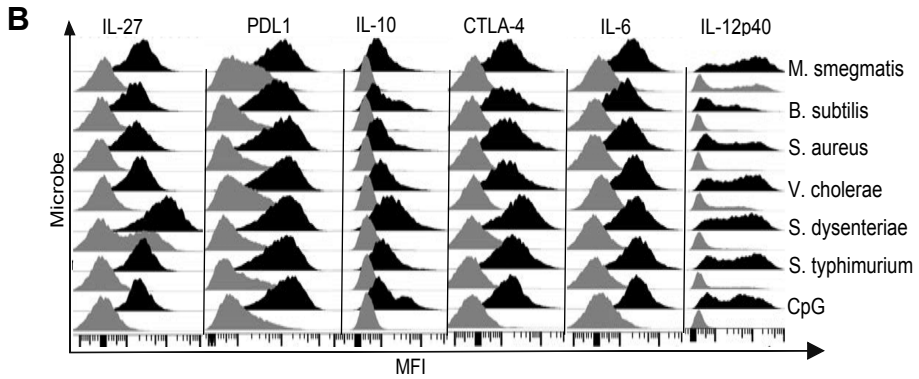

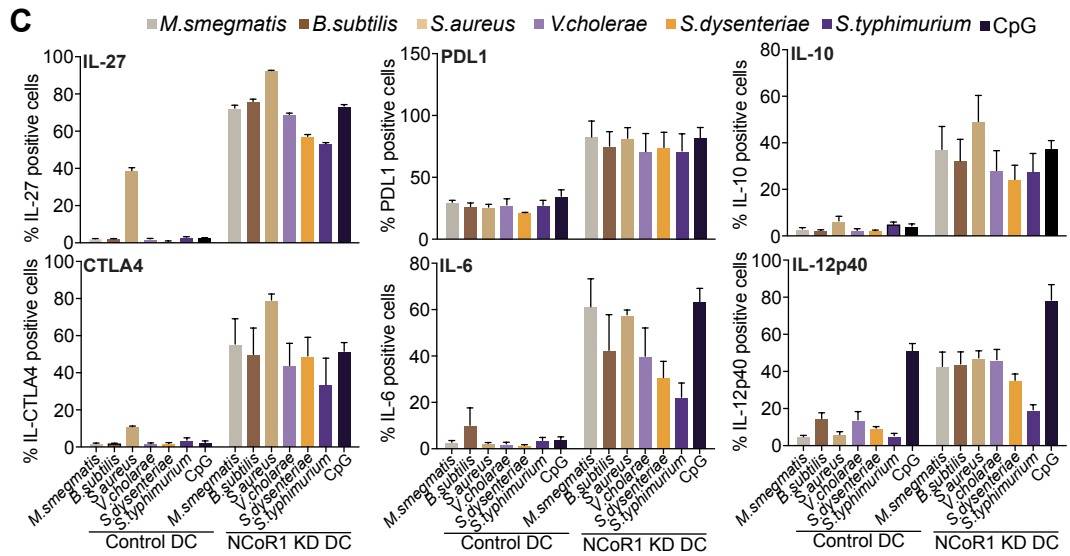

Figure S2. (Related to figure 1) NCoR1 KD cDC1 DCs develop strong tolerogenic behavior irrespective of activation by any strong TLR stimulus.

A. Scatter-plots prepared from flow cytometric analysis data showing the percentage positive cells demonstrating the expression of IL-10, IL-27, IDO1, IL-6, IL-12p40 and PDL1 in NCoR1 KD and control cDC1 DCs before and after 6h stimulation with pIC or CpG + pIC simultaneously.
B. Representative histogram plots depicting the MFI shifts for IL-27, PDL1, IL-10, CTLA4, IL-6 and IL-12p40 in NCoR1 KD and control cDC1 DC line before and after 6h challenge with heat killed gram-positive and gram-negative bacteria.
C. Bar graph depicting the percentage positive cells for IL-27, PDL1, IL-10, CTLA4, IL-6 and IL-12p40 in NCoR1 KD $CD8\alpha^{+}$ DC line as compared to control cells after 6h bacterial challenge. (n=3)

p-values are calculated using two tailed paired *t*-test. Error bars represent SEM.

*≤ 0.05, **≤ 0.01, ***≤ 0.001

Figure S3: Related to Figure 3

.

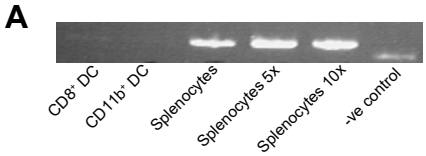

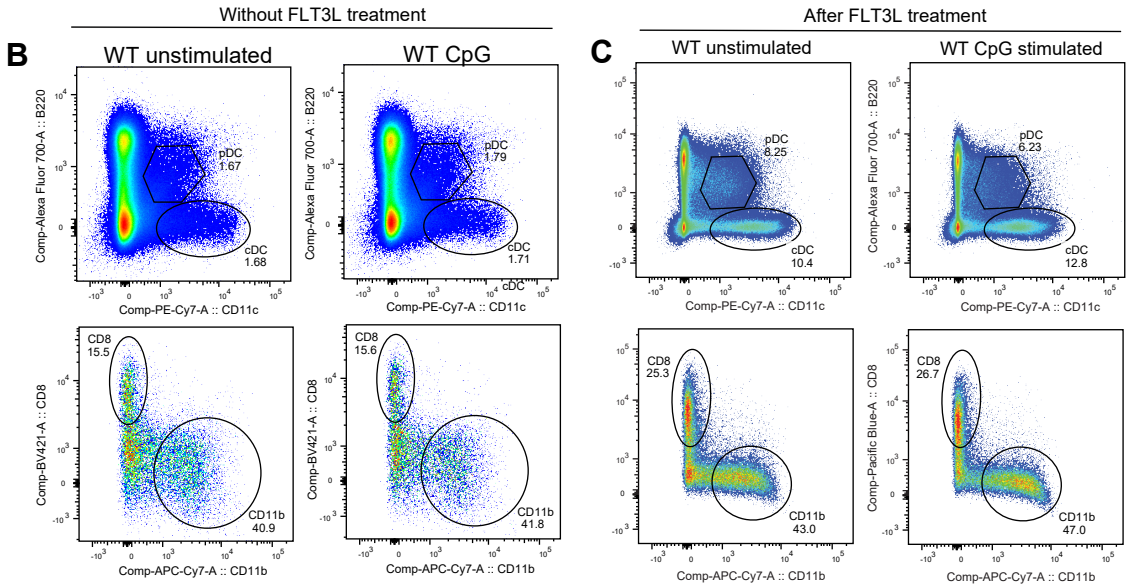

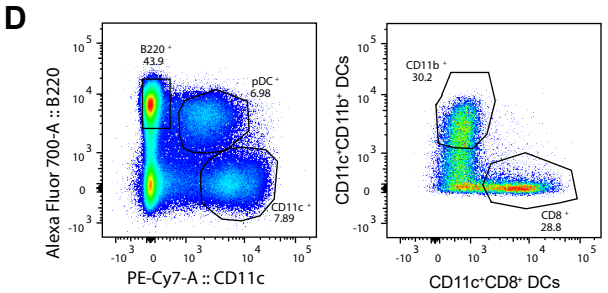

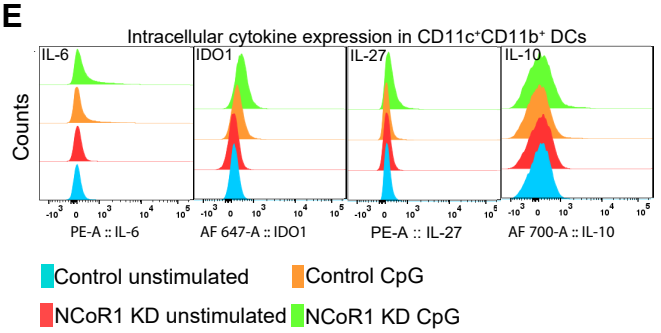

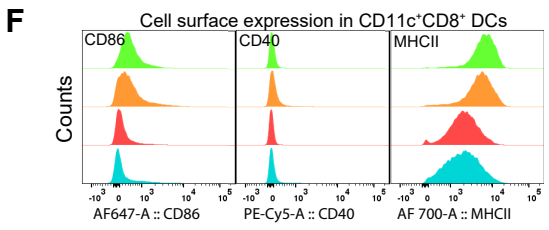

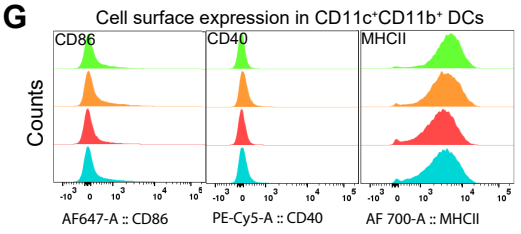

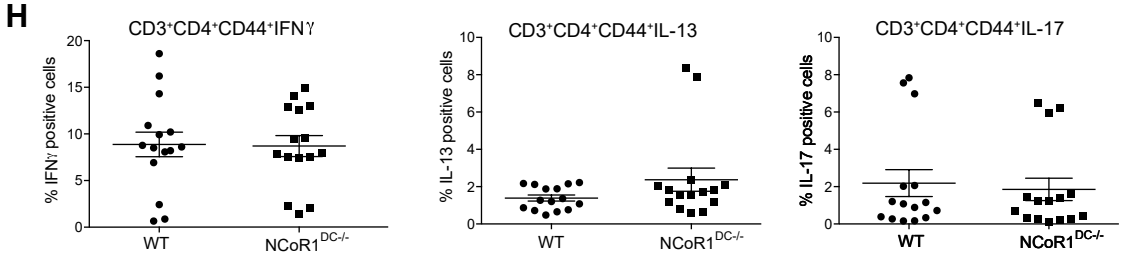

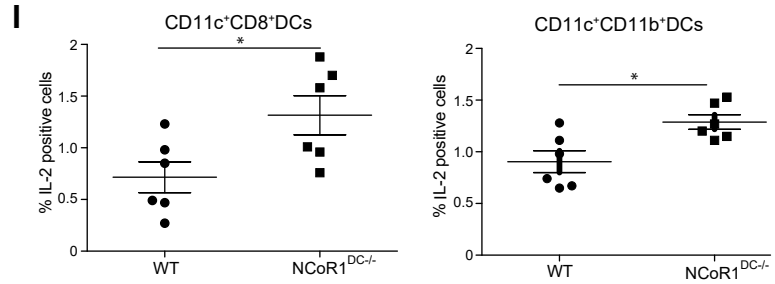

Figure S3 (Related to figure 3) CD11c^{+} DCs from NCoR1$^{DC-/-}$ mice show strong tolerogenic behavior upon CpG challenge.

A Agarose gel picture showing the presence or absence of the PCR products for the NCoR1 transcript in NCoR1$^{DC-/-}$ mice. The PCR was performed from DNA extracted from 4 x 10^5 CD8^{+} or CD11b^{+} FACS sorted DCs or splenocytes isolated from NCoR1$^{DC-/-}$ mice. Splenocytes 5X represents DNA from 2 x 10^6 Splenocytes 10X from 4 x 10^6 total splenocytes from NCoR1$^{DC-/-}$ mouse. No template control lane (-ve control) is PCR without template DNA.

B. & C.Representative dot-plots showing the percentage of pDCs, cDCs and further gated CD8^{+} and CD11b^{+} DCs in the cDC population before and after FLT3L treatment in WT and NCoR1$^{DC-/-}$ mice.

D. Dot-plots showing the gating strategy used for the flow cytometric analysis of different DC subsets from splenocytes of WT and NCoR1$^{DC-/-}$ mice.

E. Representative histograms showing the MFI differences in the intracellular expression of IL-6, IDO1, IL-27 and IL-10 in primary CD8^{+} cDCs gated in splenocytes treated with or without CpG for 6h from NCoR1$^{DC-/-}$ and WT mice. (n=6)

F. Flow cytometric analysis showing MFI shifts for cell surface markers CD40, CD86 and MHC-II in cDC1 DCs gated in splenocytes with or without 6h CpG stimulation from conditional NCoR1$^{DC-/-}$ and WT mice. (n=6)

G. Flow cytometric analysis showing MFI shifts for CD40, CD86 and MHC-II in primary cDC2 DCs gated in splenocytes with or without 6h CpG stimulation. (n=6)

H. FACS dot-plots depicting percentage of positive cells expressing IFNγ, IL-13 and IL-17 in effector T helper cell population from OVA + CpG vaccinated NCoR1$^{DC-/-}$ and WT mice. Five mice were used in each group each with three technical replicates. (n=5)

I. Flow cytometric analysis showing percent positive cells for IL-2 in cDC1 and cDC2 DCs gated in splenocytes isolated from conditional NCoR1$^{DC-/-}$ and WT mice and activated with or without CpG for 6h (n=6)

p-values are calculated using two sampled unpaired T-test. Error bars represent SEM.
*$\leq$ 0.05, **$\leq$ 0.01, ***$\leq$ 0.001

Figure S4: Related to Figure 3

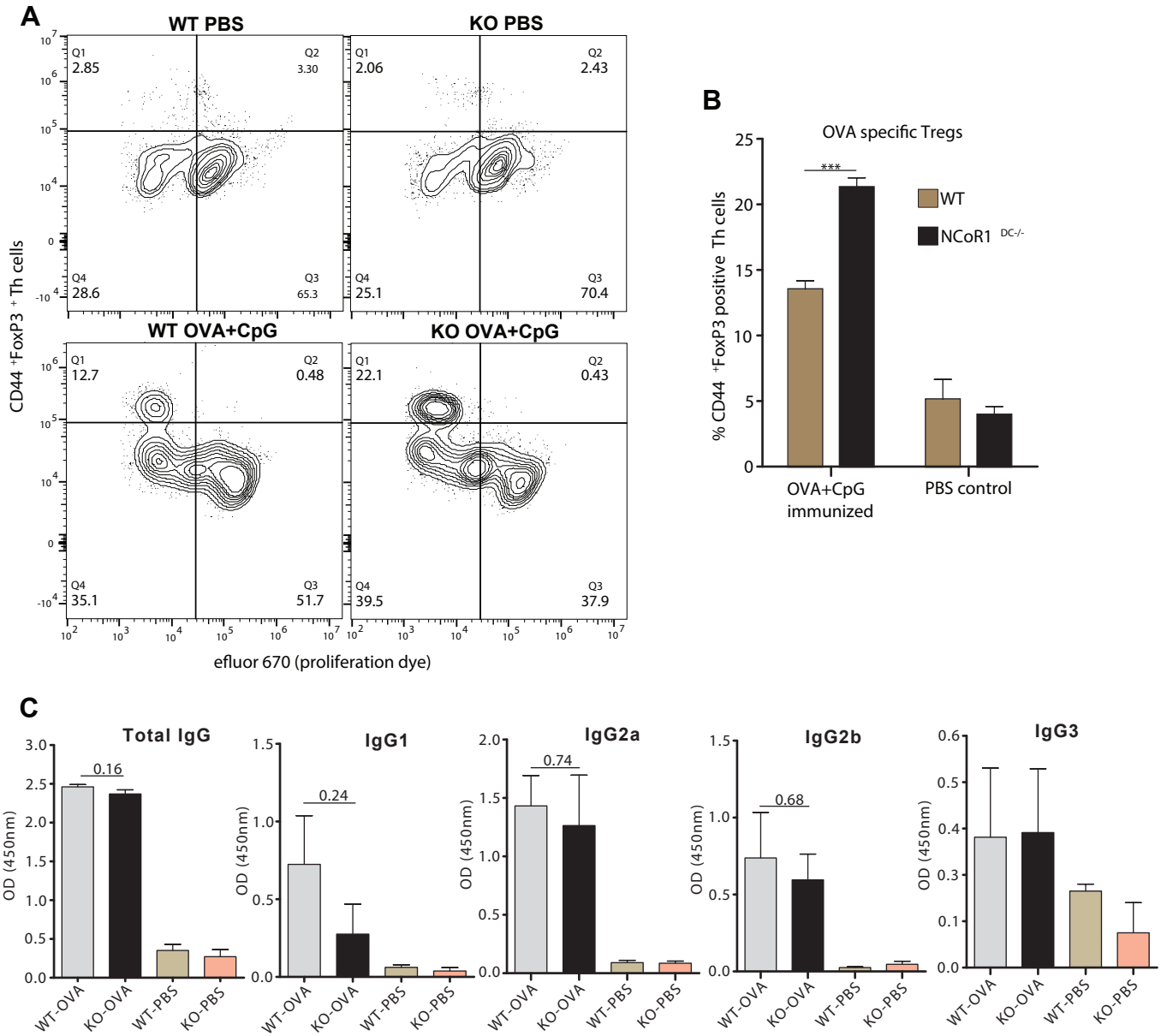

Figure S4. (Related to figure 3) T helper cell profiling of OVA+CpG immunized NCoR1$^{DC-/-}$ and WT animals.

A. FACS dot plots depicting the proliferation and percentage of FoxP3 positive population in effecter Th cells in isolated from lymph nodes of WT and NCoR1$^{DC-/-}$ OVA+CpG immunized animals. PBS immunized animals were used as controls. (n=5)

B. Bar graph showing the percentage positive FoxP3 cells in restimulated lymph node cells of WT and NCoR1$^{DC-/-}$ OVA+CpG immunized animals. PBS immunized animals were used as controls. (n=5)

C. ELISA results showing the OVA specific total IgG and isotype titres in serum of WT and NCoR1$^{DC-/-}$ OVA+CpG immunized animals. PBS immunized animals were used as controls. (n=5)

p-values are calculated using two sampled unpaired T-test. Error bars represent SEM.

*≤ 0.05, **≤ 0.01, ***≤ 0.001

Figure S5: Related to Figure 4.

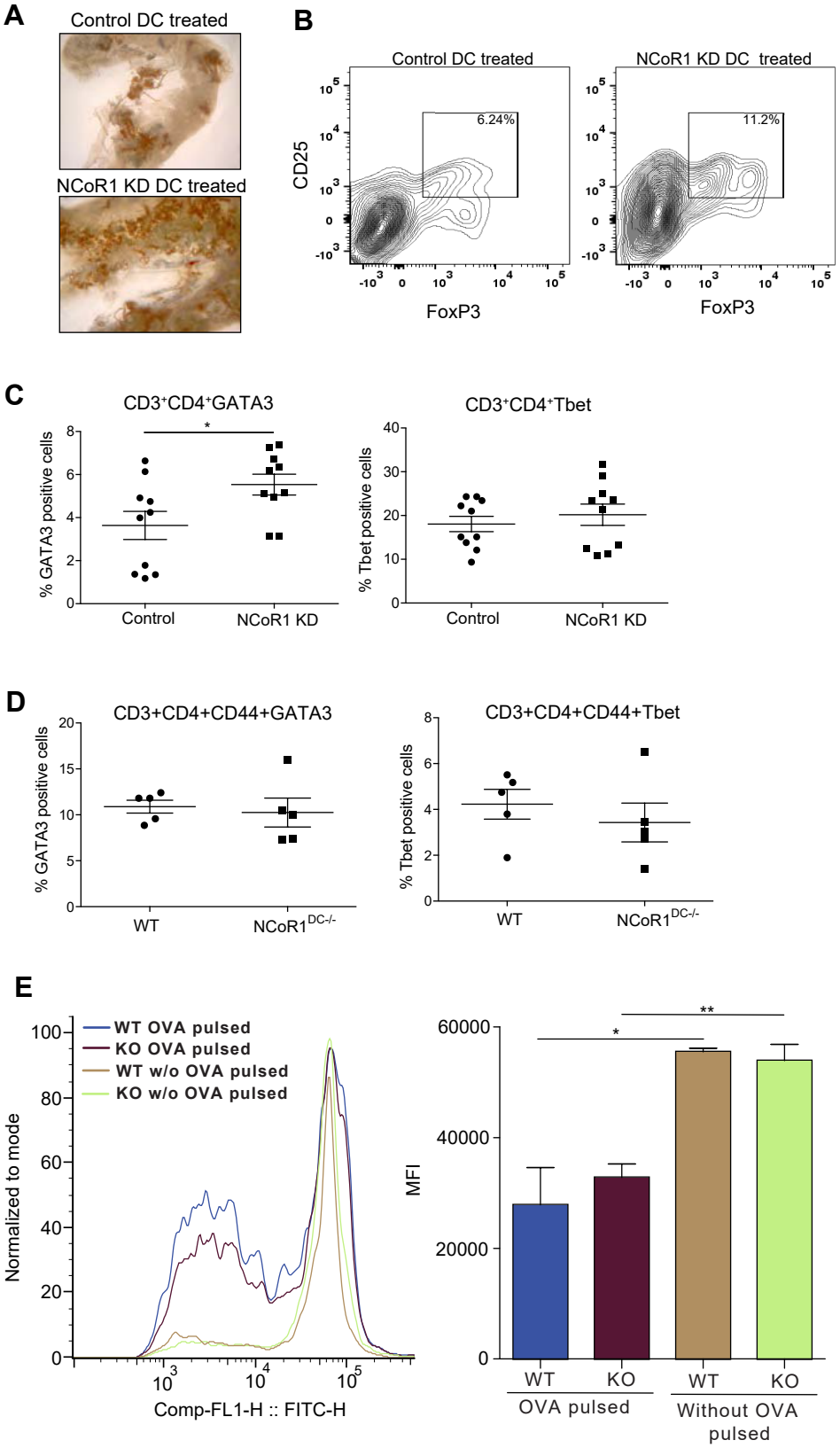

Figure S5. (Related to figure 4) NCoR1 KD/KO increases the egg and worm load by enhancing Treg population in Mesentric Lymph Nodes of helminth infected mice.

A. Representative pictures showing the helminth worms in the intestine of mice injected with CpG activated NCoR1 KD DCs as compared to control DCs. Images are representative of five mice from each group. The intestine was dissected and cut longitudinally to open it for worm counting and for taking the pictures. The images were taken from similar intestinal regions of different mice for comparison.

B. Contour-plot depicting the effector $CD25^{+}FoxP3^{+}$ Tregs in mesenteric lymph nodes (MLN) of CpG pulsed NCoR1 KD and control DC treated mice 15 days post helminth infection. (n=8)

C. Scatter-plots showing the percentage of positive T helper cells for GATA3 and Tbet from MLN of NCoR1 KD and control $CD8\alpha^{+}$ DC treated helminth infected mice after D15 (15 days) of infection. (n=10)

D. Scatter plots showing the percentage positive cells for GATA3 and Tbet producing CD4+CD44+ effector T cells from MLNs of helminth infected and CpG treated WT and $NCoR1^{DC-/-}$ mice D17 post infection. (n=5)

E. Histogram and bar plot showing the OT-II specific antigen presentation in helminth infected WT and $NCoR1^{DC-/-}$ mice (n=5)

p-values are calculated using two sampled unpaired *t*-test. Error bars represent SEM. *≤ 0.05, **≤ 0.01, ***≤ 0.001

Figure S6: Relative to Figure 6

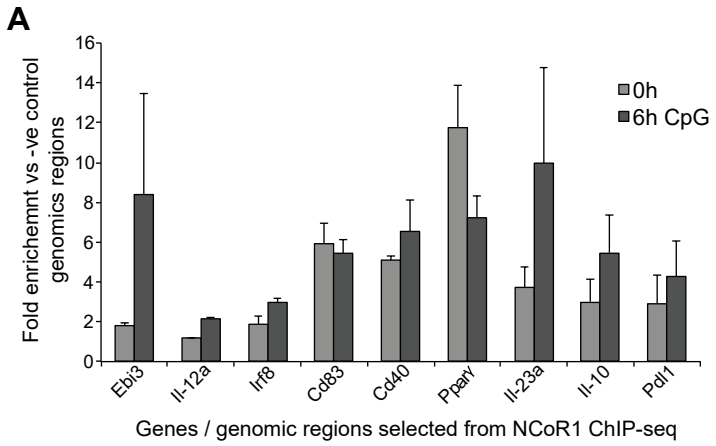

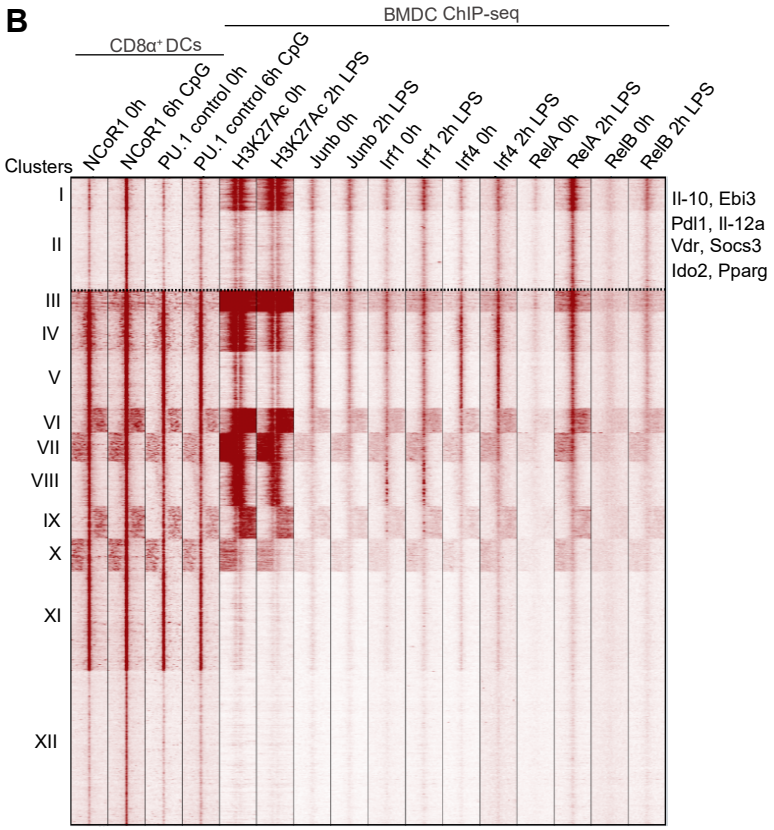

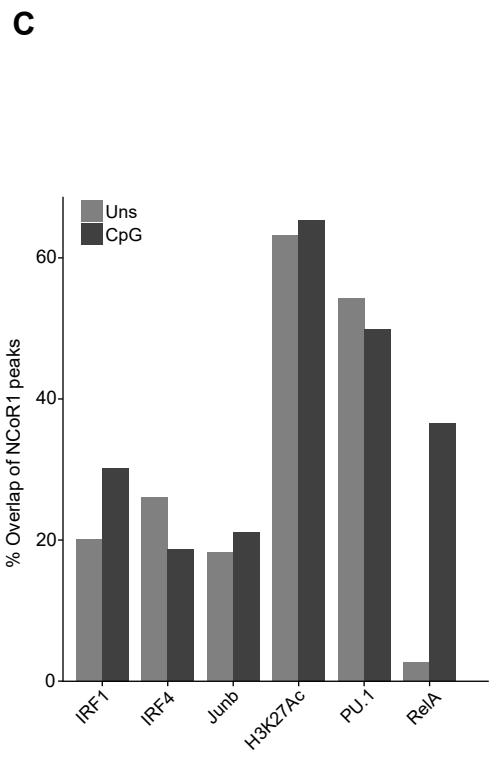

Figure S6. (Related to figure 6) PU.1 TF tethers NCoR1 to DNA in CD8α^+ DCs and NCoR1 directly represses tolerogenic genes after activation by masking the effects of activating TFs.

A. Bar plot showing the ChIP-qPCR fold change enrichment of NCoR1 at nine randomly selected genomic regions enriched in NCoR1 ChIP-seq data as compared to average of two negative control genomic regions. (n=2) Error bars shows standard deviation of NCoR1 enrichment in two independent biological replicates.
B. SeqMINER plot showing the global clustering of NCoR1, PU.1 binding at NCoR1 peaks in CpG activated CD8α^+ DCs. ChIP-seq data from unstimulated and 2h LPS stimulated primary BMDCs for H3K27ac histone mark and TFs PU.1, IRF1, IRF4, Junb, RelA and RelB was also clustered. Published and online available primary BMDC ChIP-seq data was reanalyzed using the pipeline used for the analysis of NCoR1 data.
C. Bar plot showing the percent overlap of NCoR1 with H3K27ac histone mark and TFs PU.1, IRF1, IRF4, Junb, RelA in 2h LPS stimulated primary BMDCs. Published and online available primary BMDC ChIP-seq data was reanalyzed using the pipeline used for the analysis of NCoR1 data.

Figure S7: Related to Figure 6.

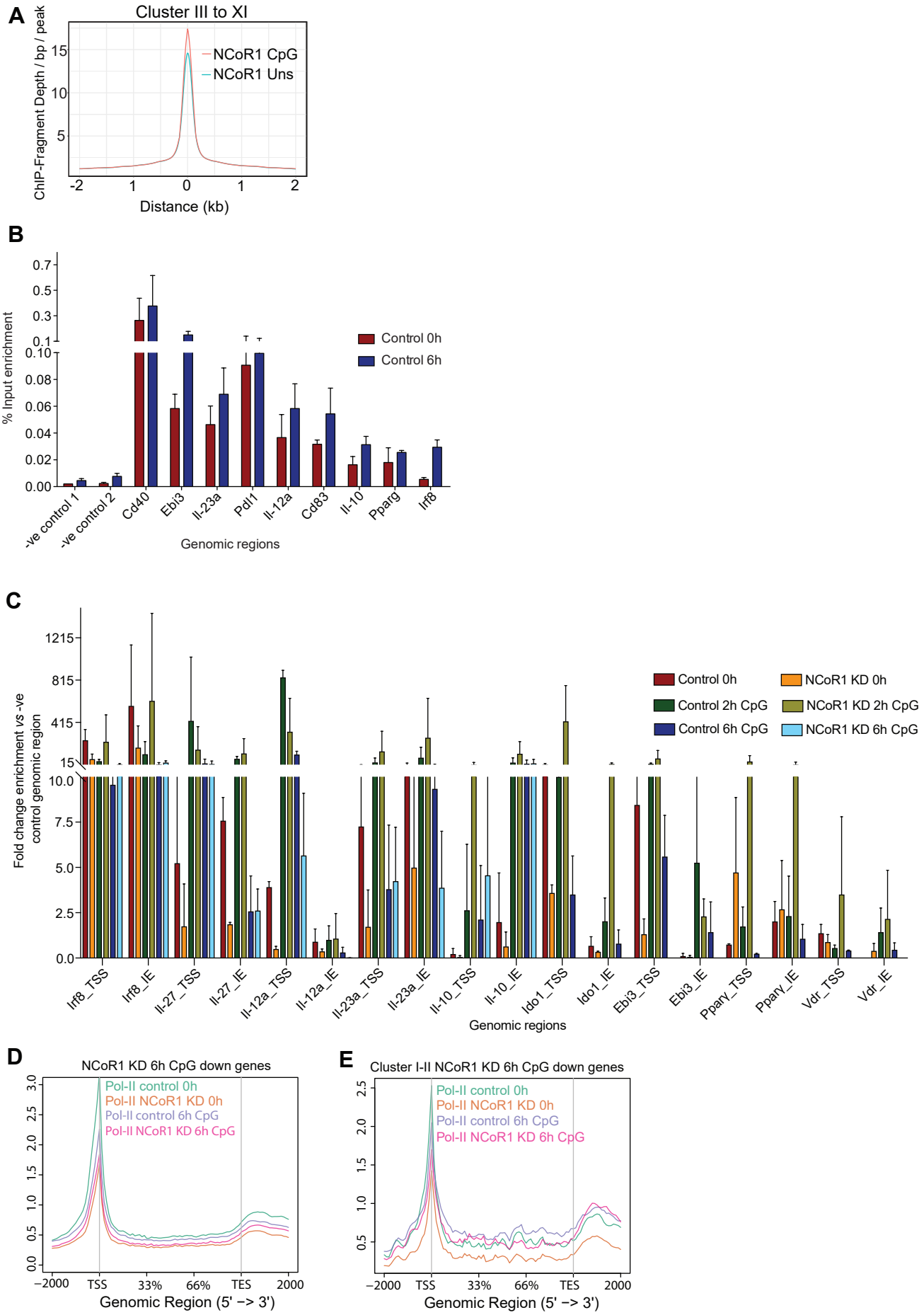

Figure S7. (Related to figure 6) NCoR1 represses PU.1 bound enhancers that are enriched for activating TFs such as RelA, IRFs, Jun after DC activation.

A. Density-plots showing the ChIP-seq intensity for NCoR1 peaks in seqminer clusters III to XI.
B. Bar plot showing the ChIP-qPCR fold change enrichment of PU.1 at nine randomly selected genomic regions enriched in NCoR1 ChIP-seq data as compared to average of two negative control genomic regions. (n=3) Error bars shows standard deviation of NCoR1 enrichment in three independent biological replicates.
C. ChIP-qPCR for RNA Pol-II in unstimulated and CpG activated (2h & 6h) control and NCoR1 KD DCs depicting the fold change enrichment of Pol-II at transcription start site (TSS) and gene body (intra-exonic, IE) of selected tolerogenic genes compared to negative control genomic region. (n=2)
D. Metagene plot depicting the RNA Pol-II profile in unstimulated and 6h CpG stimulated control and NCoR1 KD DCs for the total list of down-regulated genes in 6h CpG activated NCoR1 KD RNA-seq analysis.
E. Metagene plot showing the RNA Pol-II profile in unstimulated and 6h CpG stimulated control and NCoR1 KD DCs for the list of down-regulated genes in 6h CpG activated NCoR1 KD RNA-seq analysis and annotated to cluster I-II genomic regions

Supplementary table legends

Table S1. (Related to figure 5). The information of the CSV file containing the list of NCoR1 ChIP-seq peaks and the annotated genes in unstimulated (sheet 1) and 6h CpG activated (sheet 2) CD8α^+ DCs.

Table S2. (Related to figure 5). The information of the CSV file containing the list of differentially expressed genes significantly regulated in RNA-seq of 6h CpG challenged NCoR1 KD CD8α^+ DCs compared to control cells. Sheet-1: List of genes significantly upregulated (q-value $\leq$ 0.01 and $\geq$2 fold change) in NCoR1 KD compared to control DCs, Sheet-2: List of significantly down-regulated (q-value $\leq$ 0.01 and $\leq$2 fold change) genes in NCoR1 KD compared to control DC after CpG stimulation, Sheet-3: Genes significantly upregulated in RNA-seq list and are also bound by NCoR1 in ChIP-seq data of 6h CpG stimulated CD8α^+ DC, and Sheet-4: Genes significantly down-regulated in the RNA-seq list and are also bound by NCoR1 in ChIP-seq data of 6h CpG challenged CD8α^+ DC.

Table S3. (Related to figure 5). The information of the CSV file with the list of differentially expressed genes significantly regulated in RNA-seq analysis of unstimulated NCoR1 KD CD8α^+ DCs compared to control DCs. Sheet-1: List of genes significantly upregulated (q-value $\leq$ 0.01 and $\geq$ 2 fold change) in NCoR1 KD versus control DCs, Sheet-2: List of significantly down-regulated (q-value $\leq$ 0.01 and $\leq$2 fold) genes in NCoR1 KD compared to control KD DCs, Sheet-3: Genes bound by NCoR1 in ChIP-seq data and significantly upregulated in RNA-seq list, and Sheet-4: Genes bound by NCoR1 in ChIP-seq data and significantly down-regulated in RNA-seq list.

Table S4. (Related to figure 5). The information of the enriched pathways analysis through GeneGo Metacore analysis report CSV file with different sheets showing the list of biological pathway maps, process networks, diseases and GO processes significantly enriched for the 658 NCoR1 directly controlled and upregulated genes. ChIP-seq and RNA-seq correlation allowed identification of the genes directly controlled by NCoR1. Sheet-1: Biological pathway maps significantly enriched with their respective p-value and the genes involved, Sheet-2: Process networks significantly enriched with their respective p-value and the genes involved, Sheet-3: Diseases significantly enriched for the list of NCoR1 regulated genes with their respective p-value, and Sheet-4: GO Processes significantly enriched with their respective p-value.

Table S5. (Related to figure 5). The information of the enriched pathways analysis through GeneGo Metacore analysis report CSV file with different sheets showing the list of biological pathway maps, process networks, diseases and GO processes significantly enriched for the 439 NCoR1 unbound but upregulated genes. ChIP-seq and RNA-seq correlation lead us to identify the genes that are indirectly controlled by NCoR1. Sheet-1: Biological pathway maps significantly enriched with their respective p-values and the genes involved, Sheet-2: Process networks significantly enriched with their respective p-values and the genes involved, Sheet-3: Diseases significantly enriched for the list of NCoR1 regulated genes with their respective p-values, and Sheet-4: GO Processes significantly enriched with their respective p-values.

Table S6. (Related to figure 6). The information of the total list of genes in Excel file showing the that are annotated to cluster I-II shown in Fig. 6c and then differentially bound and regulated by NCoR1 in CpG condition and also enriched for other transcription factor PU.1 after activation. Sheet 1 shows total annotated genes whereas sheet 2 and sheet 3 shows genes that are bound and upregulated in NCoR1 KD and down-regulated after CpG activation respectively.

Table S7. (Related to figure 6). The information of the CSV file showing the list of genomic regions identified as super-enhancer (SE) or strongly repressed regions for NCoR1 and PU.1 respectively in unstimulated and CpG activated CD8α^+ DCs. We used the HOMER super enhancer discovery tool to identify the genomic regions and the genes that are showing strong enrichment (high rank for PU.1 and NCoR1). Sheet 1 and 2: Region list showing the NCoR1 strongly repressed (SR) regions and the annotated genes arranged according to their rank of repressor regions in unstimulated and CpG stimulated DCs respectively, Sheet 3 and 4: Region list showing the PU.1 super-enhancer (SE) regions and the annotated genes arranged according to their rank of enhancers in unstimulated and CpG stimulated DCs respectively.

Transparent Methods

Dendritic cell (DC) culture

The CD8α+ cDC1 and CD11b+ cDC2 DC lines were recently developed(Fuertes Marraco et al., 2012; Pigni et al., 2018).These cell lines perfectly mimic extraordinarily the immature cDC1 and cDC2 DCs isolated ex vivo from C57BL/6J mice(Fuertes Marraco et al., 2012; Pigni et al., 2018). The culture conditions were optimized for these immature DC lines. In brief, the cells were grown in IMDM medium supplemented with 10% FBS and antibiotic solution, 5 x 10-5 M β-mercaptoethanol, sodium bicarbonate, HEPES. The cells were maintained at 37°C in a humidified incubator with 5% CO2. These DCs were dissociated with a short incubation of 2-3 min in a non-enzymatic, 5 mM EDTA in 20 mM HEPES buffer. For in vitro experiments, the DCs were plated in 6-well plates at a density of 5 x 105 cells/ml overnight. The cells were then challenged with different activation media containing TLR9 agonist CpG-B, TLR3 agonist pIC, and CpG+pIC for different time points. For performing RT-qPCR analysis the cells were washed in the plate once with PBS followed by addition of RNA-later (RLT) buffer (Qiagen) for lysis of cells. The plates were then stored at -80oC until further RNA isolation and processing of samples.

Generation of stable NCoR1 KD CD8α+ and CD11b+ DCs

For generating stable NCoR1 knockdown (KD) and corresponding control DCs, lentiviral vector pLKO.1 (Sigma) containing NCoR1-specific shRNAs or control shRNA were used. Viral particles packaged with shRNA expressing transfer plasmids were produced in 293T cells using CalPhos mammalian transfection kit (Clontech) according to an optimized protocol (Barde et al., 2010) . 293T cells were transfected with transfer plasmids containing NCoR1 shRNAs or control shRNAs along with packaging plasmids (pCMVR8.74 and pMD2G). After 12-14h the culture medium was refreshed and the supernatant containing viral particles were collected after 24h in 50

ml conical tubes. The viral particle-containing culture supernatant was filtered through 0.45 µm syringe filters and preserved at -80°C in small aliquots. For transduction of shRNA containing viruses in CD8α+ or CD11b+ DC lines, the cells were plated at a density of 1.25 x 105 cells/well of 12 well plates followed by transduction with virus particles containing supernatant. The media was replaced with fresh media after 12h of virus incubation with DCs followed by addition of 1 µg/ml puromycin selection medium after 72h. The cells were puromycin selected for two to three weeks to get stable NCoR1 KD cells. The cells were also transduced with control shRNA-containing viruses to develop control cells for analysis comparisons. The efficiency of NCoR1 KD was quantified using NCoR1 gene specific primers by RT-qPCR. The shRNA that showed a significant and maximum decrease in NCoR1 gene transcript levels compared to control transduced cells were used for the further detailed study.

RNA isolation and RT-qPCR

Total RNA was isolated using RNeasy plus kit (Qiagen) according to vendor recommended protocol. The RNA concentration was estimated by nanodrop (Thermo) and then 1 µg of total RNA was used to prepare cDNA using SuperScript-III Reverse Transcriptase kit (Invitrogen). Quantitative PCR was performed using SYBR Green master mix (Roche) and PCR amplification was monitored in real-time using LightCycler-480 Instrument (Roche). Primer oligonucleotides for qPCR were designed using a universal probe library assay design system (Roche) and the primer pairs used are listed above in supplementary information. Primers were optimized for linear and single product amplification by performing standard curve assays.

Flow Cytometry (FACS)

Flow cytometric analyses of in vitro and ex vivo cultured cells were performed using routinely employed methods for FACS staining and analysis. After dissociation from

plates, the cultured cells were washed with FACS buffer (3% FCS in PBS, 5mM EDTA) followed by resuspension in surface staining buffer containing Fc receptor blocking antibody. After washing, fluorochrome conjugated antibodies for proteins of interest were added to the cells as a cocktail (see the list of antibodies for details). For intracellular (IC) staining of cytokines, the cells were first fixed with 2% paraformaldehyde followed by permeabilization using 1x permeabilization buffer (eBiosciences). The fixed cells were then resuspended in intracellular staining buffer containing Fc receptor blocking antibody and stained with fluorochrome tagged antibodies for selected cytokines. For optimal staining, the cells were incubated with antibodies for 30 min in dark at room temperature. After incubation, the cells were washed three times with FACS wash buffer and then acquired for differential expression analysis on LSRII flow cytometer (BD Biosciences). The acquired data were analyzed using FlowJo-X software (Treestar). All antibodies used in flow cytometry experiments are listed in resource table.

Bio-Plex (Luminex) assay for cytokine quantitation from cell culture supernatants

Bio-Plex assay (multiplex ELISA) was used to estimate the cytokines levels secreted in the cell culture supernatants of NCoR1 KD and control DCs before and after CpG stimulation. After culture the supernatants were stored at -80□C in small aliquots until analysis. Cytokine levels were estimated using 23-plex-mouse cytokine assay kit following the vendor recommended protocol (Biorad).

Indoleamine 2,3-dioxygenase (IDO) activity assay

IDO activity in cell culture supernatants of NCoR1 KD and control cells before and after 6h CpG stimulation was performed using the protocol described before(Feng and Taylor, 1989) . Fifty □l culture supernatants from NCoR1 KD and control CD8α+ DCs

were mixed with 30 ml of 30% trichloroacetic acid in 96 well plates followed by spin at 4000 rpm for 8 min. After centrifugation half of the supernatant was mixed with equal volume of Ehrlich reagent (0.8% p-dimethyl aminobenzaldehyde in acetic acid) for 30 min to allow conversion of L-tryptophan to L- kynurenine. The optical density (OD) of developed colored product was measured using spectrophotometer at 490 nm. Standard curve using known concentration of L- kynurenine was prepared to calculate the L- kynurenine using the observed ODs. Samples and standards were treated at the same time.

Generation of DC specific NCoR1 knockout mice (NCoR1$^{DC-/-}$)

DC specific conditional knockout (KO) C57BL/6J mice for NCoR1 gene (NCoR1$^{DC-/-}$) were generated using Cre-Lox recombination system(Birnberg et al., 2008) . Animals having Cre-recombinase driven under the minimal DC-specific CD11c promoter were used to delete the NCoR1 gene specifically in DCs(Yamamoto et al., 2011) . NCoR1fl/fl mice were crossed with CD11c-Cre mice and resulting heterozygous progenies were back-crossed for several generations to obtain pure homozygous NCoR1$^{DC-/-}$ mice. Genotyping PCRs were performed for NCoR1 and Cre gene using DNA isolated from sorted CD11c+ DCs and total splenocytes to identify the deletion status of NCoR1 gene in animals (Supplementary Fig. 3a). For getting sufficient number of DCs ex vivo from NCoR1$^{DC-/-}$ mice were treated with FLT3L serum (equivalent to 50 mg/ml FLT3L) for 10 days. Spleens were then harvested and digested with collagenase-D for 20 min at 37°C. After obtaining a single cell suspension, conventional DCs were FACS sorted using cell surface markers i.e., B220-CD11c+CD8+ and B220-CD11c+CD11b+ cells. Then DNA was extracted from 4 x 105 FACS sorted DCs for genotyping PCR. DNA was extracted using the DNeasy Blood & Tissue DNA isolation kit (Qiagen) according to the recommended protocol. After NCoR1 gene PCR, samples were loaded on a 2% agarose gel to visualize the presence or absence of PCR product. After confirmation

of the NCoR1 ablation by the absence of PCR product the experiments were performed on 6-15 weeks old sex-matched mice. For all the in vivo and ex vivo mice experiments we strictly followed the guidelines approved by the Swiss Federal and Cantonal veterinary or the ILS guidelines authorities.

For ex-vivo DC experiments using wild type (WT) and NCoR1DC-/- mice, the animals were treated with FLT3L alternatively for 8 days as described before for getting sufficient number of DCs. Single cell suspensions were made from spleen and lymph nodes of NCoR1DC-/- mice. Spleens were incubated with collagenase-D solution for 20 min at 37□C followed by mild mincing with the syringe plunger. The suspension was then treated with 1x RBC lysis buffer (Tonbo). Lymph nodes were minced into small pieces with sterile scalpel or scissors in a culture dish. Cell clumps were then passed through 70 μm strainer to obtain single cell suspensions.

Co-culture of DCs with CD4+ T cells for assessing T cell proliferation and differentiation

DC-T cell co-culture experiments were performed as described before(Smita et al., 2018). Naïve CD4+ T cells were purified from spleen of TCR-transgenic OTII mice using CD4+ T cell isolation kit (Miltenyi Biotec). NCoR1 KD and control CD8α+ DCs were seeded at a density of 20,000 cells/well in round bottom 96 well plates followed by incubation with OVA (aa 323-339) peptide with and without CpG for 2h. After 2h, purified OT-II T cells were added at the density of 100,000 cells/well (1:10 ratio). For T cell proliferation, CD4+ T cells were labeled with eFluor-670 proliferation dye (eBiosciences, Cat no: 65-0840-85) before co-culture with DCs. Proliferation rate and T helper cell differentiation into different subtypes were analyzed by FACS after 5 days. Fluorochrome conjugated antibodies specific to different T cell subtypes were used to profile T cells into Th1 (Tbet and IFNγ), Th2 (GATA3, IL-13), Tregs (CD25, FoxP3) and Th17 (IL-17). For gating effector T cell gating we used CD44 marker antibody (see

reagent list for details of antibodies).

CpG and OVA immunization to ascertain the in vivo impact of NCoR1 gene ablation on T cell differentiation

To identify the functional impact of NCoR1 ablation on T helper cell differentiation, we performed CpG + OVA vaccination. Different vaccine formulations were tested for ovalbumin (OVA), however, the most replicable method remained a simple mixture of 50 µg CpG and 10 µg OVA in PBS. NCoR1DC-/- and WT mice were vaccinated subcutaneously at the base of the tail at day 0 followed by a booster dose at day 30. Three mice from each group were used in each experiment and experiment was repeated five times. Three days after the booster injection, inguinal lymph nodes were harvested and T cell differentiation pattern into Th1, Th2 or Tregs was analyzed by flow cytometry.

OVA specific T cell response and ELISA

To examine OVA specific immune response we performed experiments as described (Alignani et al., 2005) (Maletto et al., 2002) (Semmrich et al., 2012) . In brief, we collected sera at D33 after OVA immunization from NCoR1DC-/- and WT animals to perform ELISA for OVA specific IgG titer. Elisa plates were coated with 100ug/ml of OVA (Sigma) prepared in bicarbonate / carbonate coating buffer for overnight at 4°C following five washes with washing buffer (PBS with 0.05% tween -20). Blocking was done with PBST containing 0.5% gelatin for 1h at 37°C. After five times washing, 1:10 diluted sera were added from NCoR1DC-/- and WT mice and kept for 1.5 h at 37 °C. Total IgG was detected using anti-mouse HRP conjugated IgG whereas IgG isotypes were detected using biotin labelled anti-mouse IgG1, IgG2a, and IgG2b following with anti-mouse streptavidin-HRP (Biolegend). The plates were read using ELISA reader for IgG estimation.

For OVA specific T cell proliferation and FoxP3 levels, we performed the experiment as described before (Huang et al., 2010) . In brief, cells were harvested from inguinal lymph nodes of NCoR1DC-/- and WT mice at D33 and stained with proliferation dye ef-670 (ebioscience). These stained cells were co-cultured with OVA pulsed DCs for three days. After three days, CD4 T cells were stained and analyzed for proliferation and FoxP3 levels.

Specificity for antigen presentation by DCs from WT and NCoR1DC-/- mice were examined by injecting 5 X 106 purified CD45.1+ CFSE labelled OT-II T cells in helminth infected CD45.2+ WT and NCoR1DC-/- mice at D12 of infection through tail vein. Next day 1 X 106 wild type DCs pulsed with OVA peptide or media alone were transferred through same route. After five days i.e. day 17, we took splenocytes from WT and KO mice and checked for peptide specific proliferation of FACS gated CD45.1+ cells.

Chromatin Immuno-Precipitation (ChIP) for NCoR1, PU.1, RNA Pol-II, and RelA

The ChIP for NCoR1 and TFs was performed according to the method optimized previously by Raghav and colleagues (Raghav and Deplancke, 2012). Several NCoR1 antibodies were optimized for performing NCoR1 pull-down for efficient ChIP assays and therefore in this study, we have used the same antibody(Raghav and Deplancke, 2012). For ChIP assays, 30 x 106 CD8α+ cDC1 DCs were seeded in 15 cm2 plates and prepared for ChIP before and after 2h & 6h after CpG or pIC stimulation. PU.1 and RNA Pol-II ChIPs were also performed in NCoR1 depleted and matched control DCs at similar time points. For ChIP, the cells were cross-linked using 1% formaldehyde (Sigma) for 10 min at room temperature followed by quenching the reaction using 2.5 M glycine (Sigma) for 10 min. The plates were placed on ice and the cells were scraped and collected in 50 ml conical tubes. The cells were then washed three times using cold 1 x PBS and cell pellets were stored at -80°C. At the day of ChIP experiment, the

cells were thawed on ice followed by lysis in nuclei extraction buffer (50 mM HEPES-NaOH pH 7.5, 140 mM NaCl, 1 mM EDTA pH 8.0, 10% glycerol, 0.5% NP-40, 0.25% TritonX-100) supplemented with protease and phosphatase inhibitors (Roche) for 10 min at 4°C on rocker shaker. The prepared nuclei were then washed using protein extraction buffer (200 mM NaCl, 1 mM EDTA pH 8.0, 0.5 mM EGTA pH 8.0, 10 mM Tris-HCl pH 8.0) supplemented with a protease and phosphatase inhibitors (Roche) at room temperature for 10 min. Washed nuclei were resuspended in chromatin extraction buffer (1 mM EDTA pH 8.0, 0.5 mM EGTA pH 8.0, 10 mM Tris-HCl pH 8.0 and 1% TritonX-100) supplemented with protease and phosphatase inhibitors (Roche) and incubated for 20 min on ice for equilibration. The chromatin was fragmented using a Bioruptor (Diagenode) sonicator for 30 min using high amplitude and 30s ON & 30s OFF cycles to obtain 200-500 bp size fragments. A cooling unit was used to circulate the cold water during sonication to avoid de-crosslinking because of overheating. After sonication, chromatin length was checked in agarose gel. The fragmented chromatin was centrifuged at 10,000 rpm for 5 min and then clear supernatant was collected in 15 ml conical tubes. The DNA concentration of the chromatin was estimated using a NanoDrop (Thermo) and the chromatin was diluted with ChIP dilution buffer (1 mM EDTA pH 8.0, 10 mM Tris-HCl pH 8.0 and 1% TritonX-100 containing protease and phosphatase inhibitors) to use 150 µg/ml of chromatin for each IP. BSA and ssDNA (Salmon Sperm DNA) pre-blocked protein-A sepharose (80 µl/IP) beads were added to the samples on ice and incubated for 2h to remove non-specific-binding chromatin. To the supernatant, 5 µl of rabbit polyclonal anti-NCoR1 (Abcam, cat no: ab-24552), 25 µl of anti-PU.1 (Santa Cruz, sc-390659), or RNA Pol-II (Cell signaling, 2629S) were added to immuno-precipitate the chromatin complex at 4°C overnight on rocker shaker. After the overnight incubation, 50 µl blocked protein-A sepharose beads were added to each sample and incubated for 2.5h at 4°C to pull down the respective antibody-chromatin complexes. The beads were then washed three times with low salt wash buffer (20 mM Tris-Cl pH 8.0, 150 mM NaCl, 2 mM EDTA pH 8.0, 0.1% SDS, 1%

TritonX-100) followed by two washes with high salt wash buffer (20 mM Tris-Cl pH 8.0, 500 mM NaCl, 2 mM EDTA pH 8.0, 0.1% SDS, 1% TritonX- 100), lithium chloride wash buffer (10 mM Tris-Cl pH 8.0, 0.25 M LiCl, 1 mM EDTA pH 8.0, 1% NP-40, 1% sodium deoxycholate) and Tris-EDTA (TE) buffer (10 mM Tris-Cl pH 8.0, 1 mM EDTA pH 8.0). After removing the wash buffer completely, protein-bound chromatin complexes were eluted from beads for 30 min using elution buffer (100 mM sodium bicarbonate and 1% SDS in milliQ water). The eluted chromatin was the reverse-crosslinked by incubating the eluted supernatant at 65°C overnight on a heat block after adding 8 µl of 5 M NaCl. Next day DNA was purified from the reverse cross-linked chromatin by proteinase-K and RNase digestion followed by purification using PCR purification kit (Qiagen). The purified DNA was eluted in 40 µl of elution buffer.

ChIP-/RNA-seq library preparation for Next Generation Sequencing (NGS)

For RNA-seq library preparation 2 µg of total RNA was used to isolate mRNA through magnetic beads using mRNA isolation kit (PolyA mRNA isolation Module, NEB) followed by RNA-seq library preparation using mRNA library preparation kit (NEB) strictly following the vendor recommended protocol. After library preparation concentration of libraries was estimated using qubit 2.0 (Invitrogen) and the recommended fragmentation sizes were confirmed by Bio-analyzer (Agilent). For ChIP-seq library preparation, 30 µl ChIP-DNA was processed for library preparation according to ChIP-seq library preparation recommended protocol (NEB). After library preparation and quality check, the libraries were sent to NGS service provider (Genotypic technology, Bangalore, India) for Illumina sequencing using NextSeq-500 instrument.

ChIP-qPCR validations

For experimental validation of PU.1 and RNA Pol-II ChIP-seq results, ChIP-qPCR was

performed at 0h and 6h after CpG activation of control and NCoR1 KD DCs. Enrichment of these factors at randomly selected ChIP-seq positive genomic regions/genes was calculated in comparison to negative control genomic regions. Three independent ChIP experiments were performed for PU.1 ChIP-qPCR whereas two independent biological replicates were used for RNA Pol-II validation. For RNA Pol-II ChIP-seq libraries were prepared from ChIP-DNA samples followed by qPCR for selected genomic regions annotated to TSS and intra-exonic regions of selected DC response/tolerogenic genes using 0.5ng DNA per reaction from each sample. Fold enrichment at positive genomic regions was calculated relative to negative control regions. Similarly for PU.1 1:10 diluted purified ChIP-DNA was used to perform qPCR for the selected DC response/tolerogenic genes and negative control genomic regions (-ve ctrl1 & 2). For RNA Pol-II ChIP-qPCR, the p-value significance was calculated by comparing the enrichment of positive genomic regions in NCoR1 KD as compared to control cells. Whereas in case of PU.1 as we did not observe any overall enrichment differences in ChIP-seq, therefore, the p-value significance was calculated by comparing the enrichment of positive control genomic regions compared to negative control regions in three biological replicates. The ChIP primers used are listed in reagent list in the resource table. The p-value for enrichment significance was calculated using two-tailed paired Students t-test and error bars depicted SEM in the fold change error in enrichments observed in different biological replicates.

Similarly to validate the NCoR1 ChIP-seq results, we performed ChIP-qPCR using two independent biological replicates and checked the enrichment of ten randomly selected positive control regions as compared to two negative control genomic regions. We found that all the ten positive genomic regions were >2 fold enriched compared to an average of negative control regions (Supplementary Fig. 6e). These analyses confirmed the robustness of our NCoR1 ChIP-seq data.

Electrophoretic Mobility Shift Assay (EMSA)

Previously described method and NFkB site containing probe were used for EMSA (Banoth et al., 2015) . In brief, Cells were treated with first cytoplasmic extraction buffer (10mM HEPES-KOH pH 7.9, 60mM KCL, 1mM EDTA. 0.5%NP-40, 1mM DTT supplemented with protease inhibitor) with three rounds of vortex and incubation on ice. Cytoplasmic fraction was collected and the pellet was washed once with CE buffer and then resuspended in Nuclear extraction buffer (250mM Tris-cl pH7.5, 60mM KCL, 1mM EDTA, 1mM DTT supplemented with protease inhibitor) which further subjected to three cycles of freeze-thaw. For DNA binding assay of NFkB subunits, nuclear extracts were pre-incubated with P32-labeled double-stranded NFkB oligonucleotide probe in binding buffer [20mM Tris-Cl (pH 7.5), 100mM NaCl, 20% glycerol, 2% NP-40, 1mM EDTA, 0.1mg/ml Poly dI:dC (Santa Cruz)] and NFkB subunit was marked depending on the position of shifted bands. For determining the level of NFkB in the nucleus, nuclear extract was resolved in SDS-PAGE and immunoblotted with NFkB subunit specific antibodies.

DC microbial infection assay

Total six bacterial strains were used to ascertain the immune response changes in NCoR1 KD and control DCs with live bacterial challenge for 6h. We used three gram-positive (M. smegmatis, B. subtilis, S. aureus) and three gram-negative (V. cholera, S. dysinteriae, S. typhi) bacteria. A multiplicity of infection (MOI) 3 was used to infect DCs. CpG stimulation was used as a control for comparison. After 2h of infection, the culture medium was removed and cells were washed with media followed by addition of fresh medium. Cells were then kept for 4h at 37°C in a humidified incubator with 5% CO2. For FACS analysis the cells were treated with Brefeldin-A for 4h to prevent the secretion of cytokines in the supernatant. After 6h of bacterial activation RT-qPCR and flow cytometric analysis was performed as described above. For RT-qPCR analysis, Brefeldin-A was not added to the cells.

Heligmosomoides polygyrus helminth infection in NCoR1DC-/- and WT mice

For helminth infection, NCoR1DC-/- and WT female mice were infected with 200 infective L3 larvae of H. polygyrus in PBS per mice through oral gavage. At day 10 after infection mice were treated with 50 μg CpG-1826. The feces from treated animals were collected daily for counting worm eggs in McMaster chambers. After observing a significant difference in egg count between NCoR1DC-/- and WT animals, mice were sacrificed for detailed T cell profiling of MLNs. The intestinal helminth worms were counted from the intestine of five animals from each group. The T cell differentiation into Th1, Th2, Tregs and Th17 subtypes were assessed using FACS as detailed above.

Leishmania major infection model in NCoR1DC-/- and wt mice

L. major was provided by the group Tacchini-Cottier (WHO, University of Lausanne). For infection in NCoR1DC-/- and wt mice, 3 x 106 parasites were injected in the right footpad of each mouse. Thickness difference between the right and the left footpad was measured every 4-5 days. At day 18 mice were administered 50 μg CpG intraperitoneally. At the end of the experiments, footpads and popliteal lymph nodes were harvested to measure the parasite load. Parasite loads were quantified by qPCR and T-cell differentiation profiling was performed on popliteal lymph nodes by flow cytometry (see the details above for flow cytometric analysis method).

Adoptive transfer of DCs in helminth infection mice model

For DC Adoptive transfer experiments we took 6-8 weeks old female mice and infected them with 200 infective L3 larvae/mice in PBS through oral gavage. At day 7 after infection mice were treated with 100 □g of anti-CD8b antibody/mice followed by adoptive transfer of 10 x 106 CpG pulsed NCoR1 KD and control CD8α+ DCs in sterile

PBS intraperitoneally. Two booster doses of 5 x 10^6 cells pulsed with CpG were adoptively transferred again intraperitoneally each after 48h. After adoptive transfer of DCs, the feces were collected and eggs were counted after every 24h time period using a well-optimized protocol. After observing a significant difference in egg count between NCoR1 KD treated and control animals, five mice from each group were sacrificed for detailed T cell profiling from mesenteric lymph nodes and the helminth worms were counted from the intestine of the dissected animals. The intestines were longitudinally opened and flipped to count the worms and to take pictures. The T cell differentiation into Th1, Th2, Tregs and Th17 subtypes was assessed using FACS as detailed above. This mouse experiment was performed following the animal ethical guidelines after taking due approval from the institutional animal ethics committee at ILS, Bhubaneswar, India.

Pre-processing of ChIP-seq data

Sequenced ChIP tags from NCoR1 (Input, Unstimulated, and CpG activated DCs at 6h), PU1, and RNA pol-II in control and NCoR1 KD (0h and 6h CpG stimulation) were aligned to reference mouse genome (mm10) using Bowtie2(Langmead and Salzberg, 2012) with default parameter (bowtie2 --qc-filter -t -q -x). Duplicates reads were filtered out and uniquely aligned reads were extracted using Samtools. To carry out further downstream analysis, low quality reads and duplicates were removed and uniquely aligned reads were taken in both unstimulated and CpG stimulated samples. To compare sample, NCoR1 ChIP-seq reads were down-sampled to 35 million reads using Picard tool. ChIP-seq datasets from primary bone marrow-derived DCs (BMDCs) for transcription factors PU.1, IRF1, IRF4, JunB, RelA, and active enhancer histone mark H3K27ac before and after 2h LPS stimulation(Garber et al., 2012) were downloaded from Gene Expression Omnibus (GEO6104). Reads from all the samples sequenced in different lanes were merged together then aligned to mouse (mm10)

genome as performed for NCoR1 data.

ChIP-seq peak calling and annotation

Peak calling was performed using HOMER suite (Heinz et al., 2010) . In case of NCoR1 ChIP-seq samples, peaks were called using -factor option and fold enrichment over input ChIP tag count of 4 and FDR of 0.01 was used to get significantly enriched peaks. Total peaks obtained in were filtered based on regions falling in blacklisted regions and regions with DNA copy number variation. In case of PU1, Pol-II, and primary BMDC ChIPseq data, peaks were called using –factor option for transcription factor and –histone for H3K27ac ChIP-seq. The peaks were called in these samples based on fold enrichment of 4 over surrounding 10kb region (as given in HOMER peak finding protocol).

Total enriched peaks in NCoR1 and primary BMDC ChIPseq data were annotated to nearest gene using HOMER's annotate Peaks.pl(Heinz et al., 2010) with the default option. Peak regions were divided into promoter proximal peaks based on genes annotating between -1000 to 300 (distance to TSS) and promoter distal peaks annotating to genes other than -1000 to 300.

For PU.1 ChIP-seq validations, we performed independent ChIP-seq biological replicates using wild type and empty vector transduced control DCs at 0h and 6h after CpG activation to overlap and confirm that the PU.1 binding detection is robust and consistent in control and empty vector transduced DCs in our experiments. We found a Spearman correlation of $\geq$0.8 between PU.1 ChIP-seq peaks identified by HOMER (data not shown).

Pol-II ChIP-seq data analysis

RNA pol-II ChIPseq data in control and NCoR1 KD condition (0h, 2h, and 6h of CpG stimulation) were processed in the same manner as mentioned earlier.

De novo motif analysis

We performed de novo and known motif prediction using “findMotifsGenome.pl” of Homer suite(Heinz et al., 2010) (size -100 –len 8, 10, 12). Top known motifs from JASPAR having P-value lessthan 1e-20 as well as shared at majority of peak region (% target peaks) were taken as an enriched motif at NCoR1 peaks.

RNA-Seq analysis

Raw RNA-seq reads were aligned to RefSeq gene annotation of the NCBI38/mm10 GTF file downloaded from UCSC genome browser using tophat 2.1 (Kim et al., 2013) with default parameter (tophat -o tophat_out -G mm10_refseq mm10 R1_1.fastq.gz R1_2.fastq.gz). To carry out differential gene expression study we used Cufflink 2.2.1 suite(Trapnell et al., 2010). Assembly of each transcript and expression level estimation was carried out using cufflinks. Transcripts from both the samples were merged using Cuffmerge and differential gene expressions were carried out using Cuffdiff. To retrieve significant differentially expressed gene, the raw file generated from the Cuffdiff output were filtered using q value cutoff of 0.05 and log2 (fold change) cutoff of 1 and -1 for up-regulated genes and down-regulated genes respectively.

Pathway enrichment analysis for differentially regulated genes

To identify the pathway maps, networks, GO and disease enriched for the genes that are directly regulated (upregulated or downregulated) by NCoR1 in CpG activated CD8α+ DCs, we used GeneGo Metacore analysis software program. The gene lists were uploaded in the tool and then enrichment analysis was performed as per the manual of the software. The reports were generated as CSV file and presented here as supplementary tables 5 and 6.

Overlap of NCoR1 and PU.1 ChIP-seq from CD8α+ DCs and comparison

with ChIP-seq peaks of H3K27ac and TF marks in BMDCs

To validate enrichment of PU.1 at NCoR1 bound regions in ChIP-seq, we overlapped the peak regions of PU.1 in control and NCoR1 KD DCs before and after 6h CpG activation. We also overlapped H3K27Ac, PU.1, IRF1, IRF4 and RelA ChIP-seq data from 0h and 2h LPS stimulated primary BMDCs. We calculated the percentage of NCoR1 peaks overlapping with these transcription factors (Supplementary Fig. 6c) using R package ChIP-seeker. Further, we then visualized the tag density of these factors at NCoR1 peaks using SeqMINER 1.3.3 (Supplementary Fig. 7b, c)(Ye et al., 2011). Online available raw ChIP-seq data from primary BMDCs were analyzed using a method similar to our NCoR1 ChIP-seq data to remove any bias due to analysis. BAM files generated were then used to overlap the enriched genomic regions. K-means clustering was done to cluster the genomic regions according to the similarity in enrichment. NCoR1 binding peaks in CpG was used as a reference and the genomic regions 2kb on both left and right side of NCoR1 peaks was probed for any overlap. We restricted our analysis to 12 clusters and clusters were then arranged according to their similarity. As per difference of binding pattern in clusters I and II, we annotated these regions to genes using "annotatePeaks.pl" of HOMER. The nearest annotated genes were compared to differentially expressed gene list from our RNAseq data.

Identification of super-enhancer regulatory elements bound by NCoR1 and PU.1

Total peaks in unstimulated and CpG activation condition were stitched and super-enhancer regions were identified using ROSE (Whyte et al., 2013). We ran ROSE with a stitching distance of 12.5kb and we excluded the peaks in the region of ±2000bp around the transcription start site. Super-enhancer regions were ranked based on tag density (lowest to highest).

Annotation of identified super-enhancer regions

The identified regulatory elements that are strongly repressed (SR) by NCoR1 and super-enhancer regions bound by PU.1 were annotated to nearest genes using annotatePeaks.pl of HOMER suite. NCoR1 and PU.1 signal at enhancer regions versus regions ranked by respective signal were plotted and tolerogenic genes falling in super-enhancer regions were highlighted.

Statistical analysis

The data in different figures with biological replicates are presented as the mean ± SEM. Statistical significance of the data was analyzed using two-tailed paired Student's t-test in case of cell line data whereas for animal experiments unpaired student's t-test was used to calculate significance. Data with significantly unequal variance was transformed prior to statistical analysis. For PU.1 ChIP-qPCR we calculated the p-value significance by comparing the enrichment of positive genomic regions with negative control regions, as we did not find any major change in binding before and after NCoR1 KD. In the case of RNA Pol-II ChIP-qPCR enrichment at positive genomic regions in NCoR1 KD were compared to control cells to calculate the significance. p-values are depicted in figures as * $\leq$ 0.05, ** $\leq$ 0.01 and *** $\leq$ 0.001

Data and code availability

The sequencing data (Raw data and processed files) used in this publication is submitted to the NCBI Gene Expression Omnibus (GEO; http://www.ncbi.nlm.nih.gov/geo/). The accession number for the sequence reported in this publication is GSE110423 and the authors declare that all the data supporting the findings of this study will be accessible to the readers within the article or its Supplementary information files and from the corresponding author on reasonable request.

Supplemental References:

Alignani, D., Maletto, B., Liscovsky, M., Ropolo, A., Moron, G., and Pistoresi-Palencia, M.C. (2005). Orally administered OVA/CpG-ODN induces specific mucosal and systemic immune response in young and aged mice. J Leukoc Biol 77, 898-905.

Banoth, B., Chatterjee, B., Vijayaragavan, B., Prasad, M.V., Roy, P., and Basak, S. (2015). Stimulus-selective crosstalk via the NF-kappaB signaling system reinforces innate immune response to alleviate gut infection. Elife 4.

Barde, I., Salmon, P., and Trono, D. (2010). Production and titration of lentiviral vectors. Curr Protoc Neurosci Chapter 4, Unit 4 21.

Birnberg, T., Bar-On, L., Sapoznikov, A., Caton, M.L., Cervantes-Barragan, L., Makia, D., Krauthgamer, R., Brenner, O., Ludewig, B., Brockschnieder, D., et al. (2008). Lack of conventional dendritic cells is compatible with normal development and T cell homeostasis, but causes myeloid proliferative syndrome. Immunity 29, 986-997.

Feng, G.S., and Taylor, M.W. (1989). Interferon gamma-resistant mutants are defective in the induction of indoleamine 2,3-dioxygenase. Proc Natl Acad Sci U S A 86, 7144-7148.

Fuertes Marraco, S.A., Grosjean, F., Duval, A., Rosa, M., Lavanchy, C., Ashok, D., Haller, S., Otten, L.A., Steiner, Q.G., Descombes, P., et al. (2012). Novel murine dendritic cell lines: a powerful auxiliary tool for dendritic cell research. Front Immunol 3, 331.

Heinz, S., Benner, C., Spann, N., Bertolino, E., Lin, Y.C., Laslo, P., Cheng, J.X., Murre, C., Singh, H., and Glass, C.K. (2010). Simple combinations of lineage-determining transcription factors prime cis-regulatory elements required for macrophage and B cell identities. Mol Cell 38, 576-589.

Huang, H., Ostroff, G.R., Lee, C.K., Specht, C.A., and Levitz, S.M. (2010). Robust stimulation of humoral and cellular immune responses following vaccination with antigen-loaded beta-glucan particles. MBio 1.

Kim, D., Pertea, G., Trapnell, C., Pimentel, H., Kelley, R., and Salzberg, S.L. (2013). TopHat2: accurate alignment of transcriptomes in the presence of insertions, deletions and gene fusions. Genome Biol 14, R36.

Langmead, B., and Salzberg, S.L. (2012). Fast gapped-read alignment with Bowtie 2. Nat Methods 9, 357-359.

Maletto, B., Ropolo, A., Moron, V., and Pistoresi-Palencia, M.C. (2002). CpG-DNA stimulates cellular and humoral immunity and promotes Th1 differentiation in aged BALB/c mice. J Leukoc Biol 72, 447-454.

Pigni, M., Ashok, D., Stevanin, M., and Acha-Orbea, H. (2018). Establishment and

Characterization of a Functionally Competent Type 2 Conventional Dendritic Cell Line. Front Immunol 9, 1912.

Raghav, S.K., and Deplancke, B. (2012). Genome-wide profiling of DNA-binding proteins using barcode-based multiplex Solexa sequencing. Methods Mol Biol 786, 247-262.

Semmrich, M., Plantinga, M., Svensson-Frej, M., Uronen-Hansson, H., Gustafsson, T., Mowat, A.M., Yrlid, U., Lambrecht, B.N., and Agace, W.W. (2012). Directed antigen targeting in vivo identifies a role for CD103+ dendritic cells in both tolerogenic and immunogenic T-cell responses. Mucosal Immunol 5, 150-160.

Trapnell, C., Williams, B.A., Pertea, G., Mortazavi, A., Kwan, G., van Baren, M.J., Salzberg, S.L., Wold, B.J., and Pachter, L. (2010). Transcript assembly and quantification by RNA-Seq reveals unannotated transcripts and isoform switching during cell differentiation. Nat Biotechnol 28, 511-515.

Whyte, W.A., Orlando, D.A., Hnisz, D., Abraham, B.J., Lin, C.Y., Kagey, M.H., Rahl, P.B., Lee, T.I., and Young, R.A. (2013). Master transcription factors and mediator establish super-enhancers at key cell identity genes. Cell 153, 307-319.

Yamamoto, H., Williams, E.G., Mouchiroud, L., Canto, C., Fan, W., Downes, M., Heligon, C., Barish, G.D., Desvergne, B., Evans, R.M., et al. (2011). NCoR1 is a conserved physiological modulator of muscle mass and oxidative function. Cell 147, 827-839.

REAGENT & RESOURCES	SOURCE	IDENTIFIER
Antibodies		
Anti-CD3 FITC (clone:17A2)	e-Bioscience	11-0032-82
Anti-Foxp3 PE (clone:150D/E4)	e-Bioscience	12-4774-42
Anti-mouse IL13 PE-Cyanine7 (clone:ebio13a)	e-Bioscience	25-7133-82
Anti-mouse IL13 eFluor 450	e-Bioscience	48-7133
Anti-mouse IL27p28 PE (clone:MM27-7B1)	e-Bioscience	12-7285-80
Anti-mouse IL6 PE (clone:MP5-20F3)	e-Bioscience	12-7061-81
Anti-mouse CD80 PE (clone:16-10A1)	e-Bioscience	12-0801-82
Anti-mouse CD40 PerCP-eFluor710 (clone:1C10)	e-Bioscience	46-0401-82
Anti-mouse CD274(B7-H1)/PDL1 PerCP-eFluor710 (clone:MIH5)	e-Bioscience	46-5982-82
Anti-Hu/Mo Gata-3 PE-eFlour610 (clone: TWAJ)	e-Bioscience	61-9966-41
Anti-mouse MHCII (I-A/I-E) AlexaFluor700 (clone:M5/114.15.2)	e-Bioscience	56-5321-82
Anti-Hu/Mo CD44 eFluor450 (clone:IM7)	e-Bioscience	48-0441-82
Anti-Mo/Hu CD44 PE-Cy7	e-Bioscience	25-4031-82
Anti-mouse IL10 AlexaFluor 700 (clone:JES5-16E3)	e-Bioscience	56-7101-80
Anti-mouse MHCI(H-2Kb) APC (clone: AF6-88.5.5.3)	e-Bioscience	17-5958-80
TCRb-BV510	Biolegend	109234
Anti-mouse CD3 PE (clone:17A2)	e-Bioscience	50-0032-U025
Anti-Hu/Mo Tbet PE-Cyanine7 (clone:eBio4b10)	e-Bioscience	25-5825-82
Anti-mouse CD25 APC (clone:GL-1(GL1))	e-Bioscience	20-0862-0100
Anti-mouse CD4 PE-Cyanine7 (clone:GK1.5)	e-Bioscience	25-0041-82
Anti-mouse IFN gamma APC (clone:XMG1.2)	e-Bioscience	17-7311-81
Anti-mouse IFN gamma PE	e-Bioscience	12-7311-82
Anti-mouse CD11c APC (clone:N418)	e-Bioscience	17-0114-82
Anti-mouse CD11b APC-eFluor780 (clone: M1/70)	e-Bioscience	47-0112-80
Anti-mouse IL17 APC	e-Bioscience	17-7177-81
Anti-mouse IL4 APC	Tonbo	20-7041-U100
Anti-mouse IL5 APC	e-Bioscience	504306
Anti-mouse IL13 PE-Cy7	e-Bioscience	25-7133-82
Anti-mouse CD8α eFluor450	e-Bioscience	48-4321-82
Anti-mouse CD8α PerCP-eFluor710	e-Bioscience	46-0081-80

Anti-hu/mo CD45R(B220) AlexaFluor700 (clone:RA3-6B2)	e-Bioscience	56-0452-80
Anti-mouse STAT3 PerCP-Cy5.5 (Py705) (clone:4/P-STAT3 RUO)	BD	560114
Anti-mouse IL12(p40/70)PE (clone:C15.6)	BD	554480
Anti-mouse IDO1 AlexaFluor647 (clone:2E2/IDO1)	Biolegend	654004
PE Rat Anti-Mouse IL-2	BD	554428
CD45.1 APC-eFlour780	e-Bioscience	47-0453-80
Anti-Hu/Mo CD45R(B220) AlexaFluor700(clone:RA3-6B2)	e-Bioscience	56-0452-80
CFSE	Sigma	21888
Cell Proliferation Dye eFluor™ 670	e-Bioscience	65-0840-85
H/MpERK1/2(T202/Y204) PerCP-eFluor710 (clone:MILAN8R)	e-Bioscience	46-9109-42
Phospho-NF-κB p65 (Ser536) PE	CST	5733
Rabbit polyclonal to nuclear receptor corepressor	Abcam	ab24552
Rabbit polyclonal IgG NFkB p65(C-20)	Santa cruz	SC-372
Rabbit polyclonal IgG RelB (C-19)	Santa cruz	SC-226
Mouse monoclonal IgG PU.1 (Spi-1) (B-9)	Santa cruz	SC-390659
Mouse monoclonal RNA Pol-II (Rpb1) Ab	CST	2629
Rabbit monoclonal Histone H3 (D1H2)	CST	4499S
Rabbit monoclonal beta-Actin (D6A8)	CST	8457S
Rabbit monoclonal MyD88 (D80F5)	CST	4283S
Biotin anti-mouse IgG1	**Biolegend**	**406603**
Biotin anti-mouse IgG2b	Biolegend	406703
Biotin anti-mouse IgG2a	**Biolegend**	**407103**
Biotin anti-mouse IgG3	Biolegend	406803
HRP streptavidin	**Biolegend**	**405210**
Anti-mouse IgG-HRP	abcam	Ab97023
Donkey anti-mouse IgG-HRP	Santa cruz	SC-2314
Goat anti-rabbit IgG-HRP	**Santa cruz**	**SC-2004**
NF-kB p65	CST	8242S
RelB	**CST**	**10544s**
Histone H3(D1H2)	CST	4499S
Biological samples		
Heligmosomoids polygyrus	Nicola Harris (EPFL, Lausanne)	
Chemicals, Peptides, and Recombinant Proteins		

CpG ODN 1826	Invivogen	1826
Poly I:C (HMW)	Invivogen	TLRL-pic-5
LPS EB Ultrapure	Invivogen	TLRL-3 pelps
FLT3L serum	Transgenic mice	Baerenwaldt et al., 2016
Formaldehyde solution	Sigma	252549
Glycine	Sigma	50046
TMB ELISA substrate solution	e-Bioscience	00-4201-56
Gelatin	**Sigma**	**G1393**
CD8 T cell neutralizing antibody	Hybridoma	Clone H35
Critical Commercial Assays		
RNAeasy plus mini	Qiagen	74136
Superscript III	Invitrogen	180 80 044
Lightcycler 480 sybr green master	Roche	4887352001
Lightcycler 480 multiwell plate 96,white	Roche	04 729 692 001
Bio-plex pro mouse cytokine 23-plex	BIORAD	M60-009RDPD
BCA Protein assay kit	Thermo	PI-23227
Maxi WAVE Vertical Electrophoresis System	REPLIKA BIOTECK	MV-20WAVESYS
Calphos mammalian transfection kit	Takara	631312
NEBNEXT mRna library prep master mix set for illumina	NEB	E6100S
NEBNEXT chip-seq library prep master mix set for illumina	NEB	E6240S
NEBNEXT Poly(A) mrna Magnetic isolation module	NEB	E7490S
Foxp3/Transcription factor staining buffer set kit	ebiosciences	00-5523-00
CD4+ T cell isolation kit	Miltenyi biotec	130-104-454
Experimental Models: Cell Lines		
DC 1940 CD8a+ cell line	Fuertes Marraco et al., 2012	
CD11b cell line	This paper	
Experimental Models: Organisms/Strains		
NCoR1$^{fl/fl}$ mice	Johan Auwerx, EPFL, Lausanne	
Sequence-Based Reagents		
NCoR1 shRNA1 CCGGCCTCTAATACAGGCACTTCAACTCGAGTTGAA GTGCCTGTATTAGAGGTTTTTG	Sigma-Aldrich	Clone ID: NM_011308.2-7774s1c1
NCoR1 shRNA2 CCGGCGGCATAATCTTGACAACCTTCTCGAGAAGGT TGTCAAGATTATGCCGTTTTTG	Sigma-Aldrich	Clone ID: NM_011308.2-2269s1c1

NCoR1 shRNA3 CCGGCCAATAATTGAGGGTTCCATTCTCGAGAATGG AACCCTCAATTATTGGTTTTTG	Sigma-Aldrich	Clone ID: NM_011308.2-4381s1c1
NF-KB probe for EMSA G1 5'-GCTACAAGGGACTTTCCGCTGGGGACTTTCCAGGGA GG -3' G2 5' CCTCCCTGGAAAGTCCCCAGCGGAAAGTCCCTTGTA GC 3'	IDT	
Software and Algorithms		
Bowtie2	Langmead and salzberg 2012	http://bowtie-bio.sourceforge.net/bowtie2/manual.shtml
Tophat	Kim, pertea et al. 2013	https://ccb.jhu.edu/software/tophat/index.shtml
HOMER	Heinz, benner et al. 2010	http://homer.salk.edu/homer/
Cufflink	Trapnell, williams et al. 2010	http://cole-trapnell-lab.github.io/cufflinks/manual/
SeqMINER	Ye, krebs et al. 2011	http://bips.u-strasbg.fr/
ROSE	Whyte et al., 2013	https://bitbucket.org/young_computation/rose
ChIPseeker	Yu g, wang l and he q (2015)	http://bioconductor.org/packages/release/bioc/html/ChIPseeker.html

Gene expression primers		
Gene	**Sequence**	**source**
IL12b_F	GACTCCAGGGGACAGGCTA	IDT
IL12b_R	CCAGGAGATGGTTAGCTTCTGA	IDT
IL10_F	CAGAGCCACATGCTCCTAGA	IDT
IL10_R	TGTCCAGCTGGTCCTTTGTT	IDT
IL6_F	GCTACCAAACTGGATATAATCAGGA	IDT
IL6_R	CCAGGTAGCTATGGTACTCCAGAA	IDT
Actin_F	GGCTGTATTCCCCTCCATCG	IDT
Actin_R	CCAGTTGGTAACAATGCCATG	IDT
CD80_F	TCGTCTTTCACAAGTGTCTTCAG	IDT
CD80_R	TTGCCAGTAGATTCGGTCTTC	IDT
CD86_F	GAAGCCGAATCAGCCTAGC	IDT

CD86_R	CAGCGTTACTATCCCGCTCT	IDT
CD274/PDL1_F	CCATCCTGTTGTTCCTCATTG	IDT
CD274/PDL1_R	TCCACATCTAGCATTCTCACTTG	IDT
CCL2_F	CATCCACGTGTTGGCTCA	IDT
CCL2_R	GATCATCTTGCTGGTGAATGAGT	IDT
IL2_F	GCTGTTGATGGACCTACAGGA	GCC BIOTECH
IL2_R	TTCAATTCTGTGGCCTGCTT	GCC BIOTECH
IL27_F	GCAGGGAATTCACAGTCAGC	GCC BIOTECH
IL27_R	GGACATAGCCCTGAACCTCA	GCC BIOTECH
IDO1_F	GGGCTTTGCTCTACCACATC	IDT
IDO1_R	AAGGACCCAGGGGCTGTAT	IDT
IFNb1_F	CACAGCCCTCTCCATCAACTA	IDT
IFNb1_R	CATTTCCGAATGTTCGTCCT	IDT
NCOR1_F	TATGGACCGGGTAGACCGAG	IDT
NCOR1_R	CGGTGTTTTTGTTCCACAGGAG	IDT

ChIP primers		
Gene	**Sequence**	**Source**
Negative control 1 F	TGGCACAGTGAGCAAGTAGAA	GCC BIOTECH
Negative control 1 R	GAGGAGAGCTCGAGGGTAGG	GCC BIOTECH
Negative control 2 F	CCCTTCCAAATCTGTGTTACCT	GCC BIOTECH
Negative control 2 R	TCAACCACAGAACCAAGCAT	GCC BIOTECH
IL10 F	CTGACTTCTGCCTGGGGTAG	GCC BIOTECH
IL10 R	CCCTTATCCTCAAAGTCACGA	GCC BIOTECH
PDL1 or CD274 F	GTGATGGCCCATTTCTGAG	GCC BIOTECH
PDL1 or CD274 R	CAGCTGGCCAAACTAGCC	GCC BIOTECH
IL12a F	AGCACCTGTGTCTGAGTGGA	GCC BIOTECH
IL12a R	TTGTCTTCAAAGCCTCTGTCC	GCC BIOTECH
IRF8 F	CGTCTCTTGCTGTCAGGTCA	GCC BIOTECH
IRF8 R	CCCACTTGTGAGAGGTGAGAC	GCC BIOTECH
EBI3 F	AGTTCCCTCCTCTCCCTGTG	GCC BIOTECH
EBI3 R	CTTTCCTTCCGGCTGATG	GCC BIOTECH
PPARg F	TTGTGTTGATGTCACCAGAGG	GCC BIOTECH
PPARg R	AAACCAACTTGACAATTCTAGGAAC	GCC BIOTECH
CD40_F	GAGAAACTGGGTAGGGAACTCA	GCC BIOTECH
CD40_R	AAACGGGAAAGACCACAGC	GCC BIOTECH

CD83_F	AGGACTCATTTACTCCGCAGAT	GCC BIOTECH
CD83_R	AGGTTGTCAGGGCTACTAGTGTG	GCC BIOTECH
IL23a_F	AGGCCTAGGTCGGGACAC	IDT
IL23a_R	CCCCTTCTGCAGTCTTCTGT	IDT
EBI3 TSS_ F	TGTTTCTCTCAGTTCCCTCCTC	GCC BIOTECH
EBI3 TSS_ R	GTCACTGAGCAGCTTTCCTTC	GCC BIOTECH
IDO1 TSS_ F	CAAACCCCACAGCTGACAC	GCC BIOTECH
IDO1 TSS_ R	TGAAACTGTCCCAGGTGGA	GCC BIOTECH
IL10 TSS_ F	TCAAAAATTGCATGGTTTAGAAGA	GCC BIOTECH
IL10 TSS_ R	TTCCTGGCAAAGGTTTTTGT	GCC BIOTECH
IL12a TSS_ F	CGCAGCAAAGCAAGGTAAGT	GCC BIOTECH
IL12a TSS_ R	CCTCTAGATGCAGGGAGTTAGC	GCC BIOTECH
IL23a TSS_ F	GATCTGGCTGGCTCTGTGAT	GCC BIOTECH
IL23a TSS_ R	CCGCTTAGAAGTCGGACTACAG	GCC BIOTECH
IL27 TSS_ F	CCAAGGTCTCCTGTCACCTG	GCC BIOTECH
IL27 TSS_ R	GCAGCCCCCAGTATAAGACC	GCC BIOTECH
IRF8 TSS_ F	GACCTCATCTCCCTCCTCTCA	GCC BIOTECH
IRF8 TSS_ R	AGGCCTGAGGGTCAGAAACT	GCC BIOTECH
PPARg TSS_ F	CCGAGTGTGACGACAAGGT	GCC BIOTECH
PPARg TSS_ R	CACAGGCTCCTGTCAGAGTG	GCC BIOTECH
VDR TSS_ F	TCACCCAGAACCCCCTTC	GCC BIOTECH
VDR TSS_ R	CCAGGTGCTGAGCAGTCTCT	GCC BIOTECH
EBI3 IE_ F	ACGGTGCCCTACATGCTAAA	GCC BIOTECH
EBI3 IE_ R	AGGGAGGACAGACACTCACTG	GCC BIOTECH
IDO1 IE_ F	ACTAACCTCAGCCCCGGTA	GCC BIOTECH
IDO1 IE_ R	GGTTTCTCCACATCTCAATCG	GCC BIOTECH
IL10 IE_ F	CGGAAATGATCCAGTTTTACCT	GCC BIOTECH
IL10 IE_ R	CAAATGCTCCTTGATTTCTGG	GCC BIOTECH
IL12a IE_ F	ATCACAACCATCAGCAGATCA	GCC BIOTECH
IL12a IE_ R	AGGAAGGCTTACCTGCATCA	GCC BIOTECH
IL23a IE_ F	GCCCTATCTTCCAGATCCCTA	GCC BIOTECH
IL23a IE_ R	GAGCAACTTCACACCTCCCTA	GCC BIOTECH
IL27 IE_ F	TCAGGGAAACATTGGGAAGA	GCC BIOTECH
IL27 IE_ R	CACTGGCCCTCACTAACAGAA	GCC BIOTECH
IRF8 IE_ F	CACTCAGTGGTTTTTGGTTTCC	GCC BIOTECH
IRF8 IE_ R	TGAAATAGTGGGCTGTTTAGTCAT	GCC BIOTECH

PPARg IE_ F	CAAGCCCTTTACCACAGTTGA	GCC BIOTECH
PPARg IE_ R	CAGCTCTTGTGAATGGAATGTC	GCC BIOTECH
VDR IE_ F	GTGGGGTCGTAGGTCTTGTG	GCC BIOTECH
VDR IE_ R	TCTGAGGAGCAACAGCACAT	GCC BIOTECH